Universidade do Minho
Escola de Ciências

Henrique José Ferreira Fontes

Use of an engineered exosome-like delivery platform towards colorectal cancer therapy

October 2023

Use of an engineered exosome-like delivery platform towards colorectal cancer therapy

Henrique José Ferreira Fontes

UMinho | 2023

Universidade do Minho
Escola de Ciências

Henrique José Ferreira Fontes

Use of an engineered exosome-like delivery platform towards colorectal cancer therapy

Master's Thesis
Master's degree in Molecular Genetics

Work supervised by
Doctor Débora Carina Gonçalves de Abreu Ferreira
Professor Andreia Ferreira de Castro Gomes

October 2023

DECLARAÇÃO

DIREITOS DE AUTOR E CONDIÇÕES DE UTILIZAÇÃO DO TRABALHO POR TERCEIROS

Este é um trabalho académico que pode ser utilizado por terceiros desde que respeitadas as regras e boaspráticas internacionalmente aceites, no que concerne aos direitos de autor e direitos conexos.

Assim, o presente trabalho pode ser utilizado nos termos previstos na licença abaixo indicada.

Caso o utilizador necessite de permissão para poder fazer um uso do trabalho em condições não previstasno licenciamento indicado, deverá contactar o autor, através do RepositóriUM da Universidade do Minho.

Licença concedida aos utilizadores deste trabalho

Atribuição-NãoComercial-SemDerivações CC BY-NC-ND

https://creativecommons.org/licenses/by-nc-nd/4.

ACKNOWLEDGEMENTS

Um projeto de mestrado é um longo percurso que inclui uma trajetória com inúmeras incertezas, tristezas, alegrias e muitos desafios pelo caminho. Embora a investigação possa tornar-se algo solitário, reúne o apoio e contribuições de várias pessoas, às quais desejo expressar o meu sincero agradecimento.

À minha orientadora, doutora Débora Ferreira, que merece um agradecimento especial. Agradeço a sua orientação e o conhecimento que me transmitiu durante o decorrer deste ano, aliada à sua paciência e dedicação permanente, à sua exigência crítica e essencial, e à sua boa "vibe". Tudo isto contribuiu para enriquecer cada etapa do projeto realizado e para o meu crescimento a nível pessoal.

À professora Andreia Gomes, agradecer toda a sua disponibilidade e ajuda na orientação deste projeto, onde demonstrou um interesse genuíno no meu bem-estar. As palavras que partilhou foram uma fonte de motivação e positividade.

À doutora Cátia Pereira, pela importante ajuda no início do projeto, partilhando também o seu conhecimento e contribuindo para a resolução do trabalho. Aos meus colegas de laboratório no LCCT e LBBS, agradeço a simpatia, amizade e disponibilidade para ajudar.

Aos amigos que caminharam ao meu lado desde os tempos de licenciatura e mestrado. Nelson, Nogueira, Santos e Gabriel, o meu agradecimento pelas histórias e memórias compartilhadas ao longo destes anos. Aos amigos de longa data, Afonso, Mariana e Ana, agradeço por estarem sempre lá para mim.

Por último, mas de forma alguma menos importante, aos meus pais e avós. Não há palavras suficientes para descrever o amor, o apoio e os sacrifícios que fizeram por mim. A minha jornada académica e pessoal não teria sido possível sem eles.

Cada um de vocês, desempenhou um papel fundamental, e sou eternamente grato.

"Dreams without goals are just dreams. And ultimately, they fuel disappointment.
On the road, to achieving your dreams, you must apply discipline but more importantly, consistency.
Because without commitment you'll never start,
but without consistency, you'll never finish."

- Denzel Washington

STATEMENT OF INTEGRITY

I hereby declare having conducted this academic work with integrity. I confirm that I have not used plagiarism or any form of undue use of information or falsification of results along the process leading to its elaboration. I further declare that I have fully acknowledged the Code of Ethical Conduct of the University of Minho.

ABSTRACT

Use of an engineered exosome-like delivery platform towards colorectal cancer therapy

Colorectal cancer (CRC), stands as a critical global health concern, ranking among the deadliest cancers worldwide This is mostly due to late diagnosis, as symptoms only appear in late disease stages. Efforts have been dedicated to exploring innovative and selective therapies for cancer treatment. RNA interference (RNAi) has gained significant attention for its potential in sequence-specific messenger RNA (mRNA) silencing. Small interfering RNAs (siRNAs) are promising candidates for therapeutic gene silencing., however, unmodified siRNAs have limitations that affect clinical applications. In recent years, various delivery vehicles, including exosomes, have emerged as efficient siRNA delivery systems due to their biocompatibility and low immunogenicity.

This study focused on the development of a novel treatment strategy, specifically the use of exosomes as nanocarriers for the delivery of a particular siRNA, designed to target the *PI3KCA* gene (siPI3KCA), a key player in the PAM pathway, in two distinct CRC cell lines – RKO and HCT15. Our investigation employed a multifaceted approach. Firstly, using lipofectamine, siPIK3CA was effectively delivered to the cells.

We used western blot analysis combined with real-time PCR (RT-PCR) to analyze changes in protein and mRNA levels. Specifically, we study the expressions of PI3K, Akt and mTOR in detail. Moreover, the cytotoxic effect was determined by MTT. Results showed a reduction in PAM pathway genes, mRNA and protein expression, as well as a decrease in cellular viability.

Secondly and expanding our scope, we explored exosomes - derived from HEK-293t cells. These EVs were meticulously characterized, confirming their optimal size, charge, and the presence of standard exosomal markers through techniques like nanoparticle tracking analysis, dynamic light scattering, and western blot assays. Treating CRC cells with siRNA-loaded exosomes resulted in a rapid and substantial reduction in PIK3CA, AKT, p-AKT, p-MTOR and MTOR gene and protein levels. Furthermore, cellular migration was evaluated through wound healing assay, revealing an efficient reduction in cellular motility. Altogether, these results surpassed the effectiveness of conventional lipofectamine methods in terms of speed and efficiency.

In conclusion, this investigation underscores the potential of our siRNA approach, effectively suppressing *PIK3CA* in CRC cells, leading to significant reductions in cell viability, expression and migration. Resulting in a promising avenue, to revolutionize targeted CRC therapies.

Keywords: exosomes, drug-delivery-system, *PIK3CA*, siRNA, CRC.

SUMÁRIO

Aplicação de um modelo para a terapia do cancro colorrectal através exossomas.

O cancro colorrectal (CCR) é um problema grave de saúde a nível mundial, sendo um dos cancros mais mortais em todo o mundo. Esta situação deve-se sobretudo ao diagnóstico tardio, uma vez que os sintomas só aparecem em fases tardias da doença. Têm-se investido esforços na exploração de terapias inovadoras e seletivas para o tratamento do cancro. O RNA de interferência (RNAi) tem merecido grande atenção pelo seu potencial de silenciamento do RNA mensageiro (RNAm), apesar de apresentarem limitações que afetam as aplicações clínicas. Nos últimos anos, vários veículos de entrega, incluindo exossomas, têm surgido como sistemas eficientes de entrega de siRNA devido à sua biocompatibilidade e baixa imunogenicidade. Este estudo centrou-se no desenvolvimento de uma nova estratégia de tratamento, especificamente a utilização de exossomas como nanotransportadores para a entrega de um siRNA específico, concebido para atingir o gene *PI3KCA* (siPI3KCA), um ator chave na via PAM, em duas linhas celulares distintas de CRC - RKO e HCT15. A nossa investigação utilizou uma abordagem multifacetada. Em primeiro lugar, utilizando lipofectamina, o siPIK3CA foi eficazmente administrado às células.Utilizámos a análise western blot combinada com PCR em tempo real (RT-PCR) para analisar as alterações nos níveis de proteínas e de mRNA. Especificamente, estudámos as expressões de PI3K, Akt e mTOR em pormenor. Além disso, o efeito citotóxico foi determinado pelo MTT. Os resultados mostraram uma redução nos genes da via PAM, mRNA e expressão de proteínas, bem como uma diminuição na viabilidade celular. Posteriormente, explorámos os exossomas - derivados de células HEK-293t. Estes EVs foram caracterizados, confirmando o seu tamanho, carga e a presença de marcadores exossómicos através de técnicas como a análise de rastreio de nanopartículas, dispersão dinâmica de luz e ensaios de western blot. O tratamento de células CRC com exossomas carregados com siRNA resultou numa redução rápida e substancial dos níveis de genes e proteínas PIK3CA, AKT, p-AKT, p-MTOR e MTOR. Além disso, a migração celular foi avaliada através de um ensaio de cicatrização de feridas, revelando uma redução eficaz da motilidade celular. No seu conjunto, estes resultados ultrapassaram a eficácia dos métodos convencionais de lipofectamina em termos de rapidez e eficiência.

Em conclusão, esta investigação sublinha o potencial da nossa abordagem de siRNA, suprimindo eficazmente o *PIK3CA* em células CRC, levando a reduções significativas na viabilidade, expressão e migração celular. O resultado é uma via promissora para revolucionar as terapias direcionadas para o CRC.

Palavras-chave: exossomas, sistema de distribuição de fármacos, *PIK3CA*, siRNA, CRC.

TABLE OF CONTENTS

TABLE OF CONTENTS

List of Figures

Introduction

Materials and Methods

Results and Discussion

APPENDIXES

List of tables

List of Abbreviations

AKT: protein kinase B

cDNA: complementary DNA

DDS: drug delivery systems

DLS: dynamic light scattering

DMEM: Dulbecco's modified eagle medium

DMSO: dimethyl sulfoxide

DNA: desoxyribonucleic acid

dsDNA: double-stranded DNA

EDTA: ethylenediaminetetraacetic acid

EGF: epidermal growth factor

EGFR: epidermal growth factor receptor

EVs: extracellular vesicles

FBS: fetal bovine serum

mRNA: messenger RNA

mTOR: mammalian target of rapamycin

MTT: 3-(4,5-dimethylthiazol-2-yl)-2,5-diphenyltetrazolium bromide

PAM: PI3K-Akt-mTOR pathway

PBS: phosphate buffered saline

PCR: polymerase chain reaction

PDK-1: phosphoinositide-dependent kinase-1

PI: propidium iodide

PI3K: phosphoinositide 3-kinase

PIP2: phosphatidylinositol 4,5 bisphosphate

PIP3: phosphatidylinositol 3,4,5 trisphosphate

PTEN: phosphatase and tensin homologue

RIPA: radioimmunoprecipitation assay buffer xvii

RNA: ribonucleic acid

RNAi: RNA interference

RISC: RNA-induced silencing complex

RT: room temperature

RTK: receptor tyrosine kinase

RT-PCR: real-time PCR

siRNA: small interference RNA

TEMED: tetramethylethylenediamine

WB: western blot

WHO: World Health Organization

1. Introduction

1.1 Colorectal Cancer

Cancer has become the first cause of death in high-income countries. The high prevalence of cancer and the decline in cardiovascular disease mortality explain this phenomenon [1].

On a global scale, the incidence and number of deaths are rapidly rising in low- and middle-income countries, with population growth and ageing serving as the primary causes. Increased socioeconomic development, low levels of physical activity and excessive weight due to "westernization" of lifestyles are also associated with cancer risk factors in low- and middle-income countries [2,3,4]. In 2022 alone, 19.29 million patients were diagnosed with cancer, and nearly 10 million people died of cancer [5].

Colorectal cancer (CRC) is one of the most prevalent malignancies worldwide, accounting for over 15% of all cancer cases and causing significant morbidity and mortality [6]. The incidence of colorectal cancer varies globally, with higher rates in developed countries such as the United States, Canada, Australia, and Western Europe, and lower rates in developing regions like Asia, Africa, and South America. According to the World Health Organization (WHO), there were an estimated 1.93 million new cases and 935,000 deaths from colorectal cancer in 2022, making it the third most common cancer in men and the second in women globally [7]. The 5-year survival for early-stage colorectal cancer is approximately 90%, whereas for locally advanced or metastatic cases is 71% and 13%, respectively [8,9].

In Portugal, about 10,501 new cases of colorectal cancer were diagnosed in 2020, becoming the second type of cancer with the most deaths in the country [8].

CRC results from the accumulation of genetic and epigenetic changes that disrupt the normal processes of cell growth and differentiation in the colonic epithelium [9]. These genetic changes can be inherited or acquired during an individual's lifetime and can affect a wide range of cellular pathways involved in DNA repair, cell cycle regulation, and signaling [8,9].

1.1.1 Colorectal Cancer Staging

The primary feature for estimating disease prognosis and directing the planning of patient treatment is tumour staging, which is the histologic and radiologic assessment of disease severity [10]. The most used

staging system for CRC is the TNM Staging System **(Table 1.1)** [11], which was created by the American Joint Committee on Cancer (AJCC). Three factors are taken into consideration: the degree of the primary tumour's invasion (T stage), the disease's spread to lymph nodes (N stage), and the presence of distant metastasis (M stage) [10,11,12].

Tumour classification within the TNM staging can be divided into stages 0 to IV. Stage 0 is designated when abnormal cells are found in the mucosa of the bowel wall, with the potential of becoming cancerous. Stage I describes the development of the tumour at the mucosa of the bowel wall and into the submucosa. Stage II can be further divided into stages IIA, IIB, and IIC. Cancer that has spread from the muscle layer of the bowel to the serosa is referred to as stage IIA. Stage IIB refers to further spread through the serosa, while stage IIC refers to the spread to nearby organs. Stage III describes the progression of cancer to the lymph nodes, whereas stage IV describes the progression of the disease to a distant site from the colon (metastatic disease).

While the M category is classified based on an examination of distant lesions, the N category is determined by the additional removal of lymph nodes to confirm node metastasis [10,12].

Table 1.1: TNM Classification system according to the American Joint Committee on Cancer (AJCC) colorectal cancer staging. T stage: degree of the primary tumour's invasion. N stage: disease's spread to lymph nodes. M stage: the presence of distant metastasis. Table taken from [11].

TNM Classification System			
TX	-Primary tumours cannot be assessed	**NX**	-Regional lymph nodes cannot be assessed
T0	-No evidence of a primary tumour	**N0**	-No regional lymph node metastasis
Tis	-Carcinoma in situ	**N1**	-Metastasis in 1 to 3 regional lymph nodes
T1	-Tumour invades submucosa	**N2**	-Metastasis in 4 or more regional lymph nodes
T2	-Tumour invades muscularis propria	**MX**	-Distant metastasis cannot be assessed
T3	-Tumour invades the subserosa	**M0**	-No distant metastasis
T4	-Tumour invades other organisms or structures	**M1**	-Distant metastasis

1.1.2 Colorectal Cancer Treatment

Colorectal cancer treatment decisions are mainly based on the extent of the cancer **(Figure 1.1)**. In the case of patients with early stage I and II cancers, while the tumour is still contained, surgery is the first treatment having an 80% cure rate. Once cancer has spread to nearby lymph nodes in stage II, adjuvant chemotherapy might be needed if the cancer has a higher risk of recurring due to a high-grade, more aggressive subtype. Radiotherapy can also be used in patients for whom surgery is not advised. For stage III patients, with locally advanced cancer, 50% are still cured by surgery alone. However, it is recommended to undergo adjuvant chemotherapy for 6 months after surgery [10,12,13].

In patients with distant metastasis, stage IV, surgery is unlikely to serve as a therapeutic option even with systemic chemotherapy before or after the intervention. In these patients, and in patients who relapse with metastatic disease, chemotherapy is the main treatment with or without targeted therapies to control cancer and prolong the patient's life. Otherwise, another treatment with an immunotherapy drug might be used after initial chemotherapy [11,13].

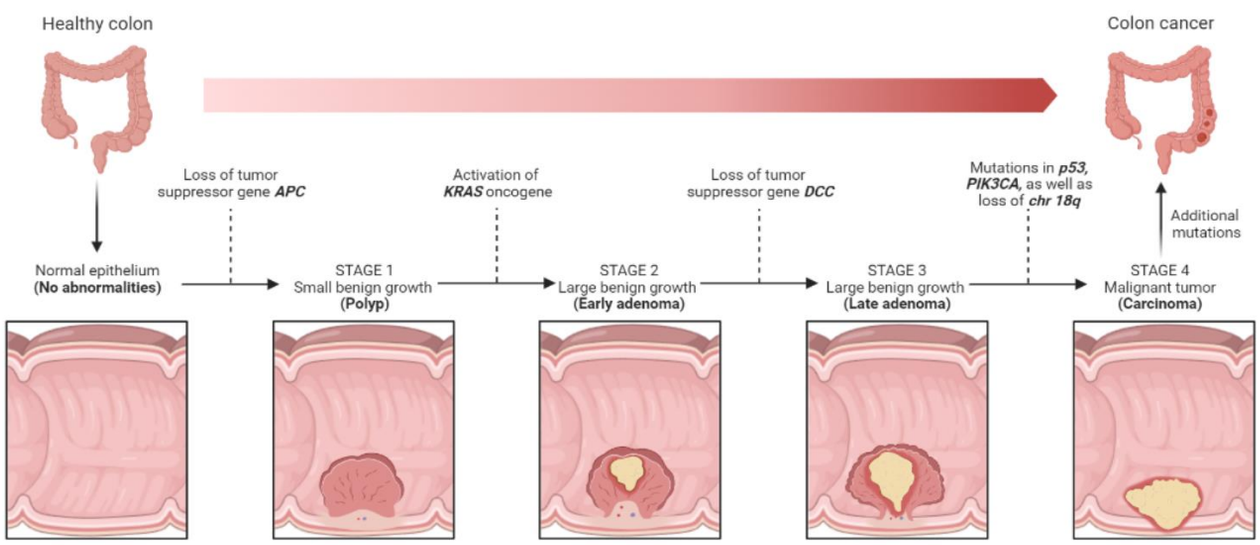

Figure 1.1: Colorectal cancer staging. Colorectal cancer begins with a mutation in the APC gene. As other tumor suppressor genes mutate, including *PIK3CA*, a larger tumor will grow and eventually become malignant. APC: Adenomatous polyposis coli. Polyp: growth of tissue that sticks out of the lining of the colon or rectum. KRAS: Kirsten rat sarcoma. DCC: deleted in colorectal cancer. Stage I: Tumors spread within muscle layers without lymph nodes or distant deposits; Stage II: Tumors spread all layers or attached to nearby tissues without lymph nodes or distant deposits; Stage III: Any stage with the involvement of regional lymph nodes; Stage IV: Any stage with distant metastasis. Adapted from [13].

Nowadays, the forefront of CRC treatment involves the utilization of targeted therapies aimed at

disrupting critical aspects of tumour growth and progression. Specifically, these therapies target two fundamental processes: blood vessel formation through the inhibition of vascular endothelial growth factor (VEGF) and the mitigation of cell proliferation through the inhibition of epidermal growth factor receptor (EGFR) [14]. While these treatments have shown promise in advanced-stage patients, there exists an exciting potential to extend their benefits to a broader spectrum of patients. However, this potential hinges on an intricate understanding of the mechanisms underpinning these drugs and a profound appreciation of the multifaceted nature of CRC biology, including its context-dependent behaviour. It is essential to underscore that patients diagnosed with stage IV metastatic CRC currently face a bleak prognosis, with a mere 14% 5-year survival rate [12,13]. Consequently, an urgent call to action is sounded for further investigation into targeted colorectal cancer therapy, with the overarching goal of ameliorating patient outcomes across all disease stages.

1.2 Targeted Therapy for Colorectal Cancer

As research in cancer biology and genomics advances, new therapeutic targets have been identified. This has inspired new therapeutics that allow an exceptional response and generally exhibit less toxic side effects than cytotoxic treatments due to their target selectivity. There are two main groups of targeted therapies: monoclonal antibodies and small molecular inhibitors [11,12,15].

Even though targeted therapy sustains hope for improvements in patient outcomes, the development of tumour resistance leading to therapy failure remains the main barrier [15,16]. Precision medicine aims to tailor CRC treatment to the specific genetic and molecular characteristics of each patient's tumour, to maximize therapeutic efficacy and minimize toxicity. Particularly, in CRC and most solid cancers there are many altered mechanisms such as AKT, growth factor receptors, *PIK3CA*, PTEN and RAS, which turn the PI3K pathway into an exceptionally interesting pharmacological target [13,16].

1.2.1. The PI3K/Akt/mTOR Pathway

The PI3K/Akt/mTOR (PAM) pathway is a crucial signaling pathway involved in various cellular processes, including cell growth, proliferation, survival, and metabolism **(Figure 1.2)**. The pathway consists of several key components, including phosphatidylinositol 3-kinase (PI3K), protein kinase B (Akt), and the

mammalian target of rapamycin (mTOR) [17,18], and plays a significant role in normal physiological functions and disease development, such as in CRC cancer [17].

1.2.2. Activation of the PI3K/Akt/mTOR Pathway

The PAM pathway **(Figure 1.2)** is activated by various extracellular signals, including growth factors, hormones, and cytokines [19]. The activation typically begins with the binding of ligands to their corresponding receptors, such as receptor tyrosine kinases (RTKs). Ligand-receptor interaction triggers the activation of RTKs, leading to the recruitment and activation of PI3K [20,21].

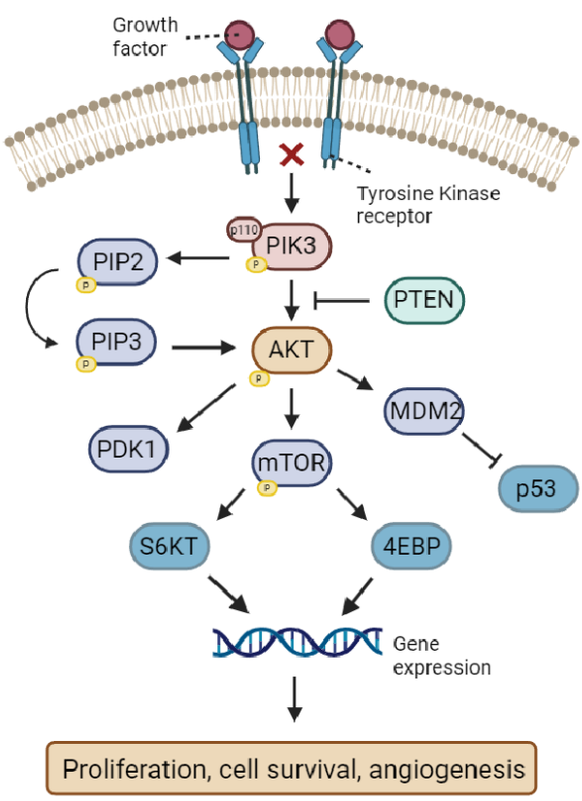

Figure 1.2: Schematic PI3K/AKT/mTOR signaling pathway representation. This pathway comprises several essential elements, including PI3K (phosphoinositide 3-kinase), Akt (protein kinase B), mTOR (mammalian target of rapamycin), PDK-1 (Phosphoinositide-dependent kinase-1), PIP2 (phosphatidylinositol 4,5 bisphosphate), PIP3 (phosphatidylinositol 3,4,5 trisphosphate) and PTEN (phosphatase and tensin homologue). Created with BioRender.com.

Activated PI3K phosphorylates, phosphatidylinositol 4,5-bisphosphate (PIP2), a membrane phospholipid, converting it into phosphatidylinositol-3,4,5-triphosphate (PIP3). PIP3 acts as a second messenger, recruiting proteins with pleckstrin homology (PH) domains to the cell membrane, including Akt. Localization of Akt to the cell membrane facilitates its phosphorylation and activation by phosphoinositide-dependent kinase-1 (PDK1). This initial phosphorylation step partially activates Akt [21,22,23].

The full activation of Akt is achieved through the phosphorylation of serine 473 by mTORC2. Activated Akt phosphorylates downstream substrates, thereby modulating cellular processes involved in cell survival, growth, and metabolism [22,23].

1.2.3. PI3K mutation and amplification in cancer

In the domain of PI3K research, it is important to note that only the class I PI3K can initiate lipid phosphorylation when stimulated by growth factors [24]. Class I PI3K is a heterodimer composed of two key subunits: the regulatory subunit p85 and the catalytic subunit p110 [25,26]. Functionally, p85 binds to phosphorylated tyrosine residues on activated receptor tyrosine kinases (RTKs) via its SH2 domain. This interaction then enables p110 to form a fully active PI3K enzyme [27].

One of the most frequently mutated oncogenes in various cancer types is *PIK3CA* [28], which encodes the p110α catalytic subunit of PI3K. *PIK3CA* mutations are commonly found in cancers such as CRC, breast cancer, lung cancer, gastric cancer, prostate cancer, and cervical cancer. These mutations typically occur near specific regions known as E545K (1633G > A, exon 9), as in cells from human colorectal adenocarcinoma (HCT-15) and H1047 (3140A > G , exon 20), as in cells from human colorectal carcinoma (RKO). E542K and E545K mutations disrupt the inhibition of p110α by p85, while the H1047 mutation enhances p110α's interaction with lipid membranes [28,29]. Although mutations in p110β, p110γ, and p110δ subunits are less frequent, their overexpression can still drive oncogenic behaviour in cultured cells [30]. In addition, CRC *PIK3CA* mutations are generally associated with KRAS mutations with RKO presenting wild-type (WT) gene and HCT-15 having a mutation in (38G > A) [31,32].

Substantial efforts have been dedicated to enhancing the effectiveness of inhibitors that target the PI3K signalling pathway. Over the past few decades, various pharmaceutical companies have undertaken the development of drugs aimed at inhibiting PI3K [33]. However, despite the approval of some PI3K inhibitors by the Food and Drug Administration (FDA), concerns persist regarding issues such as resistance

development, sensitivity markers, and toxicological effects [34]. **Table 1.2** provides a list of instances where these inhibitors have been employed in the treatment of CRC.

Table 1.2: PI3K inhibitors that target components of the PI3K/Akt/mTOR pathway, which have been assessed in clinical trials for the treatment of Colorectal Cancer. Adapted from [35-39].

Agent	Target	Disease	Phase	Reference
MSC1936369B (pimasertib). SAR245409 (PI3K and mTOR inhibitor).	-PI3K/mTOR. -MEK.	-Locally advanced or metastatic tumours. -CRC.	I	[35]
Selumetinib (MK-2206 and AZD6244)	-PI3K-AKT -RAF/MEK	-Advanced CRC. -PI3K/AKT mutation.	II	[36]
DS-7423	-PI3K/mTOR	-Advanced CRC tumors. -PI3K mutation.	I	[37]
MEN1611 in combination with cetuximab	-*PI3KCα*	-Metastatic CRC.	II	[38]
TOS-358	-*PI3KCα*	-*PIK3CA*-altered CRC	I	[39]

1.2.4 Akt Overactivation in Cancer

Akt, a pivotal protein in cancer, plays a vital role by interacting with lipids on the cell membrane. While Akt mutations in cancer are relatively uncommon, gain-of-function mutations and gene amplifications of Akt isoforms are prominent contributors to cancer progression [40]. A notable example is the Akt1 E17K mutation, which leads to constant Akt1 activity. Other activating mutations, such as E49K (Akt1) and G171R (Akt3), have also been identified, resulting in elevated levels of phosphorylated AKT (p-Akt) and heightened sensitivity to Akt inhibitors [41,42,43].

Moreover, Akt overactivation frequently stems from upstream genetic alterations in genes like *PIK3CA*, PTEN, and oncogenes such as Rasn [44]. These genetic changes enhance the expression and activity of Akt isoforms. Notably, amplifications of Akt genes, especially Akt2, are prevalent in various cancer types, including CRC [45,46]. Post-translational modifications, including lysine modifications, tyrosine phosphorylation, and others, also significantly maintain Akt hyperactivity, even when PI3K and PTEN activities remain intact. The

clinical relevance of Akt overactivation is evident in various cancer types. For instance, in CRC, Akt is often upregulated in a subset of premalignant colon lesions [45,46].

1.2.5. PTEN Loss in Cancer

In cancer, the termination of the PI3K/PIP3 signaling pathway primarily relies on the tumour suppressor PTEN [47]. PTEN's role is to dephosphorylate PIP3, converting it back to PIP2, thereby acting as a critical negative regulator of the PAM pathway, which influences cell growth and survival. Loss of PTEN function leads to sustained activation of these intracellular signals [47,48].

PTEN loss-of-function mutations are a common occurrence in various tumors. For instance, PTEN loss frequently occurs in primary and metastatic colorectal cancer, resulting in the hyperactivation of the PAM pathway and enhanced cell proliferation [49]. Interestingly, the loss of TGF-β signaling leads to the upregulation of PRL-3 and PAM pathway activation, promoting epithelial-mesenchymal transition (EMT) and tumor aggressiveness in primary CRC [50,51].

1.3 RNA interference mechanism

Another approach that has gained attention in cancer therapy in recent years is RNA interference (RNAi). RNAi is a highly conserved cellular mechanism that regulates gene expression by specifically silencing target messenger RNA (mRNA) [52]. It involves the use of small RNA molecules, including microRNAs (miRNAs) and small interfering RNAs (siRNAs), to mediate post-transcriptional gene silencing [52,53].

The RNAi mechanism, represented in **Figure 1.3**, begins with the synthesis or introduction of small RNA molecules into the cytoplasm of the cell. These small RNAs can be exogenously introduced as siRNAs [54,55,56]. Regardless of their origin, these small RNAs share a common processing pathway.

siRNAs can be chemically synthesized or introduced into the cell through exogenous delivery methods [57,58]. These siRNAs are typically designed to be double-stranded RNA molecules with specific sequences that are complementary to the target mRNA [58,59]. Upon entering the cytoplasm, Dicer also processes siRNAs, resulting in small duplexes of approximately 20-25 base pairs [60].

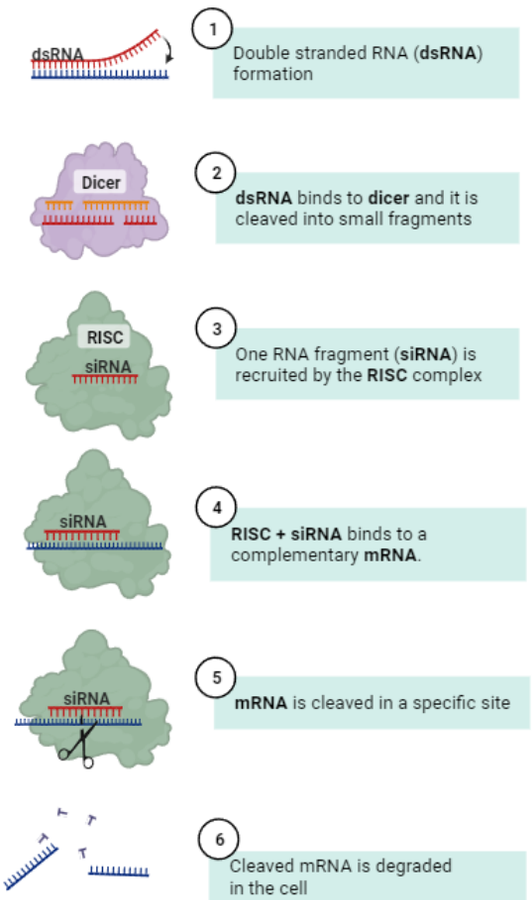

Figure 1.3: The mechanism of RNA interference. Within the cell's cytoplasm, double-stranded RNA (dsRNA) binds with the Dicer enzyme, breaking it down into smaller fragments. The complementary strand is then transported and paired with the RISC protein. This facilitates the binding of the matching mRNA transcript to the complementary strand, leading to the cleavage and subsequent degradation of the mRNA. Therefore, this process effectively inhibits protein synthesis. Created with BioRender.com.

siRNAs can be chemically synthesized or introduced into the cell through exogenous delivery methods [58]. These molecules are typically designed to be double-stranded RNA with specific sequences that are complementary to the target mRNA [58,59]. Upon entering the cytoplasm, Dicer also processes siRNAs, resulting in small duplexes of approximately 20-25 base pairs [60].

These molecules are loaded into the RNA-induced silencing complex (RISC), which contains Argonaute proteins as its key components [60,61]. Within the RISC, the guide strand of the small RNA molecule is preferentially selected and serves as a recognition element for target mRNA binding [62].

The RISC-guide RNA complex scans the cytoplasm for target mRNAs that contain complementary sequences to the guide RNA [63]. Once a complementary target mRNA is recognized, the RISC-guide RNA complex binds to the mRNA, leading to either translational repression or mRNA degradation, depending on the degree of complementarity [64,65]. Translational repression typically involves inhibiting translation initiation, while mRNA degradation involves endonucleolytic cleavage of the mRNA [66,67].

The RNAi mechanism, particularly the use of siRNAs, has become a powerful tool in functional genomics research and holds great potential for therapeutic applications [67]. siRNAs can be designed to specifically target disease-related genes, offering a promising approach for treating various diseases, including viral infections, genetic disorders, and cancers [66,67,68].

1.3.1 siRNA design

The design of siRNA molecules involves careful consideration of various parameters to ensure specificity, potency, and efficient target gene knockdown [69].

One of the key considerations in siRNA design is the selection of the target region within the mRNA. Typically, siRNAs are designed to target the coding region of the mRNA, specifically aiming for highly conserved sequences that are essential for gene function [69,70]. Avoiding regions with high sequence variability or known polymorphisms is important to ensure target specificity.

The length and composition of siRNA molecules also impact their effectiveness. The standard length of siRNAs is around 20-25 nucleotides, with a preference for 21 nucleotides [70]. The siRNA duplex consists of a guide strand and a passenger strand. The guide strand, usually the one with less thermodynamic stability at the 5' end, is responsible for target mRNA recognition and binding [71]. The passenger strand, also known as the antisense strand, is usually less loaded into the RISC and can be degraded or dissociated [71,72].

The selection of the guide strand is critical for siRNA functionality. The guide strand should have higher thermodynamic stability at the 5' end to ensure proper loading into the RISC [73]. Additionally, the guide strand should have a reduced potential for off-target effects, as unintended binding to non-target mRNAs can lead to unintended gene silencing [72,73].

Another important consideration in siRNA design is the avoidance of immune stimulation. siRNAs with specific sequence motifs, such as high guanine-cytosine (GC) content or repetitive sequences, can trigger innate immune responses [73]. Careful sequence analysis and avoidance of known immune stimulatory motifs are essential to prevent undesirable immune activation.

Several computational algorithms and software tools have been developed to aid in siRNA design, incorporating various criteria such as target accessibility, thermodynamic stability, and off-target prediction [73,74].

1.3.2 siRNA delivery

siRNA delivery is crucial to harnessing the potential of RNAi for therapeutic applications. Despite the powerful gene-silencing capabilities of siRNA molecules, their effective delivery to target cells remains a challenge. The delivery systems must protect siRNAs from degradation, facilitate their cellular uptake, and enable their release into the cytoplasm where the RISC can engage the target mRNA [73,74,75].

Various approaches have been explored for siRNA delivery, including viral and non-viral delivery systems. Peer *et al.* [75] and Zabner *et al.* [76] discussed the use of viral vectors, such as lentiviruses and adenoviruses, which exhibit high transduction efficiency and the ability to deliver siRNAs to a wide range of cell types. However, safety concerns associated with viral vectors limit their clinical applications [75].

Turning to non-viral delivery systems, Kanasty *et al.* [77] extensively studied lipid-based nanoparticles (LNPs). They highlighted LNPs' capacity to encapsulate and protect siRNAs, enhance cellular uptake through endocytosis, and facilitate their release into the cytoplasm.

In the domain of transfection, lipid-based transfection reagents, as described by Yin *et al.* [78] form complexes with siRNAs, enabling their efficient delivery into cells. As explained by Yin *et al.* [78] synthetic cationic lipid DOTMA spontaneously formed small, uniform liposomes that were capable of efficient encapsulation and delivery of RNA to various mammalian cell lines.

Other non-viral delivery approaches for siRNA delivery's, discussed by Yhee *et al.* [79] and Chakraborty *et al.* [80] include polymeric nanoparticles (NPs) and inorganic NPs. Polymeric NPs, exemplified by polyethyleneimine (PEI) and polylactic-co-glycolic acid (PLGA), efficiently encapsulate siRNAs and offer tunable properties for improved delivery [79]. Inorganic NPs, such as gold and mesoporous silica, as explored by Chakraborty *et al.* [80] provide unique features for siRNA delivery, including surface modification for targeting specific cells or tissues. Additionally, peptide-based delivery systems, as discussed by the previous researchers utilize cell-penetrating peptides or ligand-targeted peptides to enhance cellular uptake and achieve specific targeting of siRNAs [79,80]. Various NPs categories have been explored as promising vehicles for siRNA delivery, each with its own set of advantages and disadvantages. **Table 1.3** provides an overview of these NPs groups, their applications as drug delivery systems (DDS), and further details about their respective advantages, disadvantages, and practical examples.

Table 1.3: Overview of different nanoparticle categories, their utility as drug delivery systems (DDS), along with their respective advantages, disadvantages, and several practical examples. Adapted from [75–80].

DDS Approach	Advantages	Disadvantages	Examples
Lipid-based nanoparticles	-High transfection efficiency -Versatile for delivering various types of nucleic acids (DNA, RNA, siRNA). -Can be surface-modified for targeted delivery.	-Limited cargo capacity -Potential toxicity at high concentrations. -Stability issues during storage	-Liposomes -Cationic lipids -Micelles -Emulsions -Solid lipids
Viral vectors	-Efficient gene delivery -Long-lasting effects -Targeted delivery -Stable expression -Well-characterized	-Immune response -Limited cargo capacity -Insertional mutagenesis -Safety concerns	-Adeno-associated virus -Lentiviral vectors
Polymeric nanoparticles	-Controlled release -Biodegradable -Versatile	-Lower transfection efficiency compared to some other methods -Complexity of synthesis	-PLGA nanoparticles -Chitosan nanoparticles
Inorganic particles	-High stability -Controlled release -Enhanced permeation	-Potential toxicity -Limited transfection efficiency for certain particles	-Gold nanoparticles -Magnetic nanoparticles
Peptide-based	-Specific targeting -Low immunogenicity -Biocompatibility	-Limited cargo capacity -Lower transfection efficiency -Challenges instability	-Cell-penetrating peptides (CPPs) -TAT peptide

To overcome the challenges associated with siRNA delivery, researchers have also explored combinatorial approaches. For example, utilizing a combination of different delivery systems or incorporating

additional functional components, such as targeting ligands or stimuli-responsive elements, can enhance siRNA delivery efficiency and specificity [81].

As we explore siRNA delivery, it is crucial to develop new strategies for therapies. While the methods we've discussed show potential, there's growing interest in exosomes for changing and revolutionising siRNA delivery.

1.4 Exosomes

Exosomes, a subtype of extracellular vesicles (EVs), have gained significant attention in recent years due to their unique biological properties and potential applications in various fields. These small vesicles, typically ranging from 50 to 150 nanometers in diameter, are secreted by most cell types and play a crucial role in intercellular communication [82]. Their ability to transfer bioactive molecules, including proteins, lipids, and nucleic acids, between cells has led to a large amount of research in understanding their functions and discovering their therapeutic potential.

Exosomes are formed through a complex process of intracellular trafficking and membrane budding. They originate from the endosomal compartment, where an early endosome matures into a multivesicular body (MVB) through the inward budding of its limiting membrane [82,83]. This budding process results in the formation of intraluminal vesicles (ILVs) within the MVB. Subsequently, the MVBs can either fuse with lysosomes, leading to the degradation of their contents or fuse with the plasma membrane, releasing the ILVs into the extracellular environment, as exosomes [84].

These EVs carry a cargo of proteins, lipids, and various types of nucleic acids. Their proteome, lipidome, and RNA content can depend on the cell of origin and its physiological or pathological state. The presence of specific proteins, such as tetraspanins (CD63, CD9, CD81) and Alix, is often used as markers for exosome identification [83]. Moreover, exosomes are enriched in various RNA species, including mRNA, siRNA, and long non-coding RNA (lncRNA) [82,83]. Upon uptake, exosomes can modulate the behaviour of recipient cells through multiple mechanisms. For instance, exosomal proteins can activate cell signaling pathways, influencing cell proliferation, differentiation, and immune responses [83,84].

These findings align with recent advances in Exosome-based pharmaceutical carriers, as discussed by Torchilin in a comprehensive review [81]. Yáñez-Mó *et al.* [82] highlighted the biological properties and physiological functions of EVs, shedding light on the significance of exosomes in intercellular communication. Colombo *et al.* [83] delved into the biogenesis, secretion, and intercellular interactions of exosomes and other

extracellular vesicles, providing valuable insights into their formation and function. Moreover, van Niel *et al.* [84] contributed to our understanding of the cell biology of extracellular vesicles, further emphasizing their role as mediators of cellular communication.

1.4.1 Exosome Uptake by Cells

Exosome uptake can occur through multiple mechanisms, each influenced by various factors such as cell type, microenvironment, and exosome cargo. The two primary pathways of exosome internalization are endocytosis and membrane fusion. In endocytosis, exosomes are engulfed by recipient cells through different mechanisms, including phagocytosis, macropinocytosis, and clathrin-mediated endocytosis [85].

For instance, a study by Robbins *et al.* [85] demonstrated that exosomes derived from mesenchymal stem cells were taken up by neighboring fibroblasts through clathrin-mediated endocytosis, facilitating the transfer of specific growth factors.

Once internalized via endocytosis, exosomes are enclosed in endosomal compartments, and their cargo is gradually released into the cytoplasm or targeted to specific organelles [85,86]. In the study conducted by Wu M *et al.* [86] it was shown that exosomes containing miRNAs were internalized by neural cells via macropinocytosis, leading to the subsequent regulation of target genes.

Moreover, membrane fusion allows exosomes to direct contact with the plasma membrane of recipient cells, as represented in **Figure 1.4**, enabling the delivery of their cargo into the cytoplasm [86 87]. In a study by Groot Kormelink T *et al.* [87] exosomes derived from tumour cells were found to fuse with the plasma membrane of neighboring immune cells, leading to the transfer of immunomodulatory proteins and the alteration of immune responses.

Combining these characteristics through the transfer of specific siRNAs, exosomes can regulate the gene expression of recipient cells, influencing key cellular pathways, such as the PAM pathway.

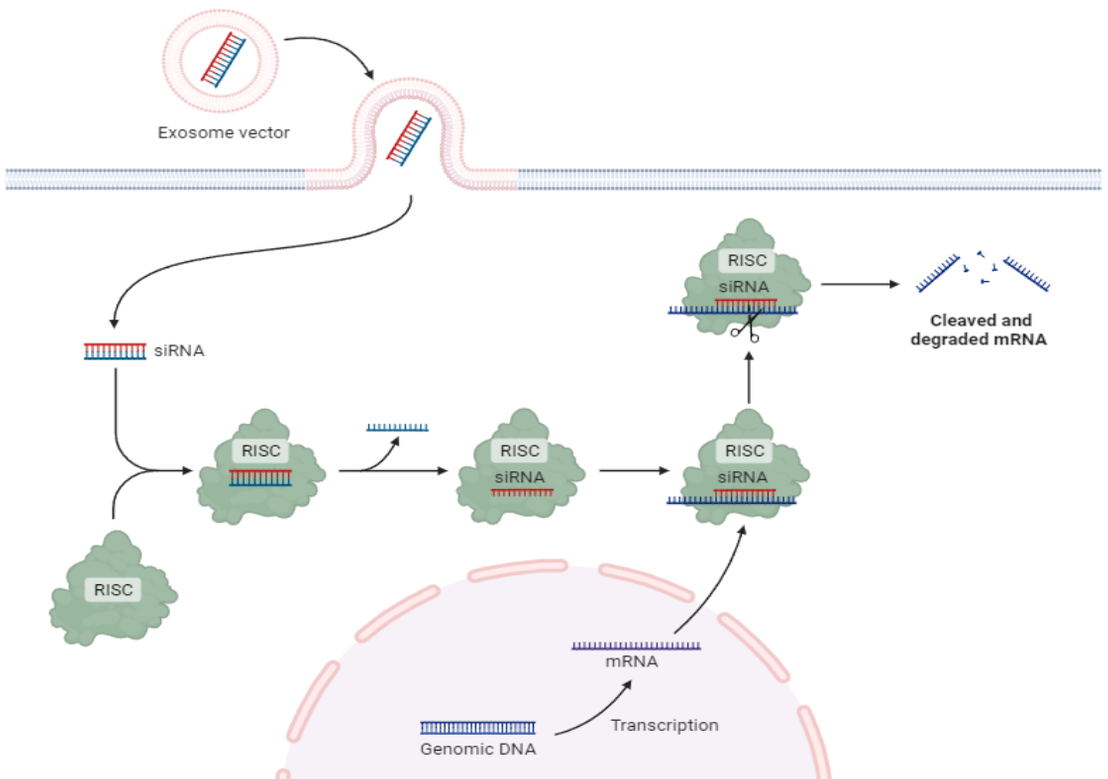

Figure 1.4: The diagram illustrates the process of exosome uptake through the cell membrane, followed by the release of siRNA into the cytoplasm. Exosomes, serve as carriers for siRNA, facilitating its delivery to the RISC complex within the cell. RISC: RNA-induced silencing complex, siRNA: small interfering RNA, mRNA: messenger RNA. Created with Biorender.com

1.4.2 Exosomes as a delivery system for siRNA

The previously cited characteristics of exosomes, make them attractive candidates for therapeutic applications for siRNA delivery. They have inherent stability, as their membrane protects the encapsulated siRNAs from enzymatic degradation and harsh extracellular conditions [83]. Moreover, exosomes can be modified with targeting ligands to facilitate specific cellular uptake and enhance the delivery of siRNAs to desired cell types [84-88].

The use of exosomes as siRNA delivery vehicles offers several advantages. Firstly, exosomes are derived from natural sources and are generally well-tolerated, reducing the risk of immune responses or toxicity associated with other delivery systems [89]. Secondly, exosomes exhibit high stability and can efficiently protect siRNAs during circulation, enhancing their bioavailability and targeting potential [89,90]. Thirdly, exosomes possess intrinsic cell-targeting abilities, allowing them to selectively deliver siRNAs to specific cell populations [89,90,91].

To utilize exosomes for siRNA delivery, various methods have been employed to load siRNAs into exosomes. These methods include electroporation, incubation, chemical conjugation, exosome engineering and direct transfection of donor cells with siRNAs, which results in the encapsulation of siRNAs into exosomes during their biogenesis [88,92,93,98,99].

For instance, Wang *et al.* [92] modified exosomes with RGD peptide and incubated them with DOX to achieve drug loading. The 131I-labeled exosomes could target tumor cells due to the presence of the targeting peptide RGD, thus, demonstrating dual antitumor strategies of internal irradiation and chemotherapy.

On the other hand, it is important to note that Kooijmans *et al.* [93] highlighted a critical consideration in siRNA loading into exosomes. Their study revealed challenges associated with electroporation-induced siRNA precipitation, emphasizing the need for refinement in loading techniques to optimize siRNA encapsulation efficiency.

The loading efficiency and stability of siRNAs within exosomes can be further enhanced through modifications such as chemical conjugation or genetic engineering [94,95]. Ohno *et al.* [96] conducted a remarkable study where the researchers harnessed the potential of exosomes as carriers for antitumor siRNA. By systemically injecting exosomes targeted to EGFR, they successfully delivered the therapeutic siRNA to breast cancer cells. This research exemplified the versatility of engineered exosomes in the realm of cancer therapy, offering the promise of more targeted and effective treatments [96].

Furthermore, exosomes can be modified to enhance their targeting capabilities [96-99]. Lee J *et al.* [98] found that incubating synthetic azide-bearing liposomes with donor cells has the intriguing effect of prompting these cells to release exosomes that carry azide groups on their lipid membranes. Following this, the bioconjugation process with targeting peptides through controlled click reactions was observed to significantly enhance the tumour-targeting capabilities of these exosomes. Finally, Cui G-h *et al.* [99] demonstrated that chemical conjugation of the exosomal surface serves a dual purpose – it enables not only targeted drug delivery but also the targeted delivery of active exosomes. By displaying an RVG peptide ligand linked to DOPE on the surface of mesenchymal stem cell (MSC)-derived exosomes, they significantly enhanced the binding of these exosomes to the cortex and hippocampus following intravenous administration. This, in turn, effectively prevented memory deficits in an animal model of Alzheimer's disease.

Examples are highlighted in **Table 1.4** and describe the remarkable versatility and potential of exosome-based delivery in a range of therapeutic applications. They highlight the need for optimization and engineering approaches to maximize the effectiveness of exosome-based delivery systems, which have the potential to revolutionize the field of drug delivery and precision medicine.

Table 1.4: This table summarizes various strategies for encapsulating small interfering RNA molecules within exosomes. Each encapsulation method offers unique advantages and strengths, as well as specific limitations and drawbacks. Understanding these characteristics is essential for selecting the most suitable method for siRNA delivery, considering factors such as cargo type, loading efficiency, and potential cellular impacts. [88,92–99].

Form of Encapsulation	Advantages	Disadvantages	References
Electroporation	- High loading efficiency -Allows for precise cargo loading - Suitable for various cargo types	- May cause siRNA precipitation -Requires optimization of parameters	[93] [88]
Incubation	- Simple and cost-effective method -Minimal cellular stress -Gentle on exosomes and cargo	- Lower loading efficiency compared to electroporation	[92]
Direct Transfection of Donor cells	- Facilitates encapsulation during - Potential for specific cargo targeting	- Limited cargo types due to dependence -May alter cellular physiology	[98]
Chemical conjugation	-Enhanced stability of siRNAs -Allows for controlled release -Versatile for various cargoes and modifications	-May require additional purification steps -Some conjugation methods may affect exosome integrity	[99]
Genetic engineering	-Precise control over cargo content -Potential for tailored exosome properties -high specificity in cargo selection	-Time consuming and technically challenging -May introduce genetic alterations in donor cells	[98]

In conclusion, exosomes offer a compelling platform for siRNA delivery. Various loading methods and modifications enable precise cargo delivery in cancer therapy. Challenges like optimizing loading techniques

and ensuring siRNA stability call for ongoing research [100]. As exemplified in Table 1.5, exosome-based siRNA delivery holds immense promise across diverse therapeutic applications. Advancements in this field have the potential to revolutionize drug delivery and drive personalized treatments, emphasizing the importance of continued research and engineering efforts.

2. Materials and methods

2.1 Cell culture procedure

The human colorectal adenocarcinoma RKO (ATCC CRL-2577) and carcinoma HCT15 (ATCC CCL-225) cell lines and the human embryonic kidney cells HEK-293t (ATCC CRL-3216) were used.

RKO and HEK-293t were cultured on tissue culture flasks in complete Dulbecco's Modified Eagle Medium (DMEM, Biochrom) supplemented with 10% (v/v) Fetal Bovine Serum (FBS, Biochrom), and 1% (v/v) of penicillin/streptomycin (P/S) antibiotic (Biochrom). The CRC cell line HCT-15 was cultivated on complete Roswell Park Memorial Institute (RPMI, Biochrom) supplemented with 10% (v/v) FBS and 1% (v/v) of penicillin/streptomycin (P/S) antibiotic.

Cells were cultured under aseptic conditions in tissue culture flasks at 37 °C and in a 5% CO_2 / 95% humidified air atmosphere, at a Hera cell incubator. When 90% confluence was reached, cells were washed with filtered phosphate-buffered saline (PBS) 1x pH 7.4 (137 mM NaCl, 2.7 mM KCl, 10 mM Na_2HPO_4, and 1.8 mM KH_2PO_4.), and detached with trypsin (Biochrom) from the flask. Cells were counted in a hemocytometer.

2.2. siRNA transfection

Cellular transfections were conducted using siRNAs to modulate target gene expression. The *PIK3CA* gene was specifically addressed utilizing a pre-established and validated siRNA sequence from Sigma Aldrich (siPIK3CA: 5'- UUCGCACCACCUCAAUAAG-3').

On the first day, RKO and HCT-15 cells were seeded in a 6-well tissue culture plate at the seeding density of $3.0x10^5$ cells per well 24 h before transfection. The next day, when the seeding confluence reached approximately 50% confluence, the medium was removed and 750 µL of serum-free DMEM was added to the wells. As shown in **Figure 2.1**, Lipofectamine RNAiMax Reagent (Thermo Fisher Scientific) and siPIK3CA (25 nM / 50 nM final concentration) solutions were prepared separately. For the Lipofectamine mix, 3.5 µL of the solution was added to an microtube followed by adding 121.5 µL of Opti-MEM (Thermo Fisher Scientific) reduced serum culture medium per well. For the siRNA mix, 5 µL of 10 µM siRNA solution was added to an microtube followed by 120 µL OptiMEM. In the end, 250 µL of combined siRNA with Lipofectamine was added to the respective well and incubated for 72 h.

For the transfection using 96 well plates, 200 µL of complete medium was added with 1.0 *x* 10^4 cells, distributed by respective wells, and then incubated overnight at 37 °C with 5% CO_2 in a humid environment. The previous day, two individuals MasterMix were prepared. The first was made with 0.5 µL Lipofectamine RNAiMax reagent with 24.5 µL Opti-MEM and the other one was prepared with siRNA (25 nM and 50 nM), adding 0.5 µL Lipofectamine RNAiMax reagent with 24.5 µL Opti-MEM per well. The subsequent actions were as previously mentioned. The combined MasterMix was added in 10 µL to the corresponding wells and incubated for transfection at 37 °C and 5% CO_2, for the respective time points of 24 h, 48 h, 72 h, 96 h and 120 h.

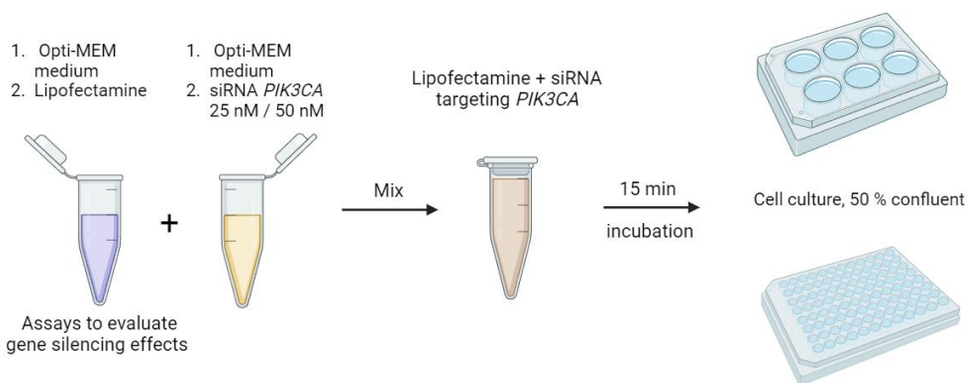

Figure 2.1: Schematic representation of the transfection procedure using Lipofectamine and siRNA *PIK3CA.* Created with BioRender.com

2.3. Evaluation of protein expression through Western Blot

The levels of protein expression were evaluated using Western Blot, allowing the identification of specific proteins, separated by size through gel electrophoresis. These proteins were then transferred to a polyvinylidene difluoride (PVDF) membrane allowing the visualization of bands and the level of protein expression through a ChemiDoc XRS image system.

2.3.1 Cell lysis method

Cell lysate procedure is crucial in Western blotting as it enables the extraction, separation, and detection of proteins of interest.

Following cell transfection (described in section 2.2), the medium containing the transfected cells was collected and placed in a tube on ice (every step from here onwards is crucial to be on ice). The cells were washed with PBS 1x at 37 °C, and trypsin was used to detach them. The non-adherent cells were then mixed with the collected medium. Each well was washed with PBS 1x again, and all the suspensions were transferred to the Falcon tubes on ice.

The tubes were centrifuged at 100 *x* g, 4 °C for 10 min, the liquid part was removed, and the pellet was resuspended in ice-cold PBS. After another centrifugation at 100 *x* g, 4 °C for 5 min, the supernatant was discarded, and the cells were resuspended in supplemented radioimmunoprecipitation assay buffer (RIPA buffer) containing 50 mM Tris-HCl (Fisher Scientific) pH 7.5, 150 mM NaCl, 2 mM EDTA, 1% NP-40 (Sigma Aldrich) supplemented with inhibitors 20 mM NaF (Sigma Aldrich), 20 mM Na_3VO_4 (Sigma Aldrich), 1 mM $C_2H_2FO_2S$ (Sigma Aldrich), 4% protease inhibitor (Alfa Aesar). The cell suspensions were incubated on ice for 20 min and then centrifuged at 2,200 *x* g at 4 °C for 15 min. The resulting supernatant was transferred to a new microtube and stored at -80°C.

This assay was equally employed to assess changes in protein expression levels induced by Exos-siPIK3CA, enabling the identification of specific proteins and the quantification of their abundance at 6 h.

Post-transfection, following section 2.2, we collected the medium containing transfected cells, followed by washing and centrifugation. The cell pellet was resuspended in PBS 1x and subsequently in a supplemented RIPA buffer. After incubation and centrifugation, protein concentration was determined using the BCA protein assay.

To quantify the protein concentration in the cell lysates, we used the BCA protein assay following the manufacturer's instructions (Thermo Fisher Scientific). The protein concentration in μg/ml was determined by comparing absorbance values (562 nm) to a standard curve generated **(Figure A.1,** in Supplementary Information) using known concentrations of bovine serum albumin (BSA, Sigma-Aldrich).

2.3.2. Preparing the SDS-Polyacrylamide gel electrophoresis (SDS-PAGE)

The separation of proteins was carried out using SDS-PAGE gels. The gel preparation involved the following steps: preparing a 10% separating gel using 40% Acrylamide (Panreac), 1.5 M pH 8.8 Tris buffer, 10% sodium dodecyl sulfate (SDS) (Thermo Fisher Scientific), 10% ammonium persulfate (APS) (VWR), and 0.1% Tetramethylethylenediamine (TEMED) (NZYTech), and a 4% stacking gel using 40% Acrylamide, 0.5 M pH 8.8 Tris buffer, 10% SDS, 10% APS, and 0.1% TEMED.

For the cellular protein samples, 30 μg of protein was mixed with 4x Laemmli Sample Buffer (LSB),

(which is composed of 65.8 mM pH 6.8 Tris-HCl Buffer, 2.1% SDS, 26.3% Glycerol and 0.01% of β-Mercaptoethanol with Bromophenol Blue in a 1:4 ratio). The mixture was heated at 95 °C for 5 min before being added to the gel wells.

For the exosome samples, 30 μg of exosome protein were mixed with supplemented RIPA buffer in a concentration ratio of 2:1. Samples were previously sonicated using an ultrasound bath for 25 sec, kept on ice for 15 min and then mixed with LSB in a concentration ratio of 1:4. The exosome lysates were then incubated at 95 °C for 5 min.

Subsequently, the cell lysate samples were loaded into the wells of the SDS-PAGE gel and subjected to electrophoresis using Tris-Glycine-SDS buffer (TGS 1x) at 60 V for 30 min followed by 200 V for 1 h.

2.3.3. Transferring the Gel

The samples were transferred from the SDS gel to a PVDF membrane (Macherey-Nagel) using a semi-dry transfer method. The membrane was activated with methanol before the transfer. The transfer involved soaking sponges and blotting paper in transfer buffer (500 mM Glycine, 50 mM Tris-HCl, 20% methanol, 0.01% SDS) and sandwiching the gel and membrane between them. The assembled transfer cassette was placed using the Trans-Blot Turbo Transfer System (Bio-Rad) in a semi-dry condition. The transfer was carried out at 2.5 amp, 25 volts for 10 min.

2.3.4 Blocking and antibody incubation

After the transfer, the membrane was washed with Tris-buffered Saline with 1% Tween (Millipore) (TBST 1x). To minimize non-specific binding, the membrane was blocked with 5% non-fat milk (0.25 g in 5 mL 1x TBST) or with 3% BSA (0.15 g in 5 mL 1x TBST), for phosphorylated antibodies, for 90 min at room temperature with agitation. Primary antibodies were diluted in 3% BSA in TBST 1x and incubated with the membrane overnight at 4 °C with agitation. The antibodies used in this experiment are listed in **Table 2.1** After incubation, the membrane was washed three times for 10 min with TBST 1x.

The membrane was then incubated with the appropriate secondary antibody for 1 h at room temperature. Subsequently, the membrane was washed three times for 10 min with TBST 1x. The protein bands were detected using a chemiluminescent substrate (Clarity Western ECL Substrate, Bio-Rad), which was prepared by mixing ECL reagent A and ECL reagent B in a 1:1 ratio. The membrane was covered with

the substrate solution, and the detection was performed using the ChemiDoc XRS+System (Bio-Rad). The intensity of the bands was subsequently quantified using ImageJ software.

Table 2.1: Antibodies used and respective dilutions in Western Blot Analysis.

ANTIBODY	DILUTION	REFERENCE
PI3 KINASE P110A	1:1000	4249S, Cell Signaling
AKT1	1:200	sc-5298, Santa Cruz
MTOR	1:200	sc-517464, Santa Cruz
PHOSPHO-AKT	1:1000	Ser473, Cell Signaling
PHOSPHO-MTOR	1:1000	Ser2448, Cell Signaling
CD9	1:1000	ab223052, Abcam Plc
CD63	1:1000	ab134045, Abcam Plc
CD81	1:500	sc-166029, Santa Cruz
ALIX	1:500	sc-53540, Santa Cruz
ANTI-B-ACTIN	1:40000	A5441, Sigma Aldrich
ANTI-RABBIT HRP	1:3000	ab205722, Abcam Plc
ANTI-MOUSE HRP	1:3000	ab10015289, Abcam Plc

2.4 mRNA expression evaluation

mRNA expression analysis is pivotal in molecular genetics research, providing insights into gene regulation within biological systems. This section provides a brief overview of the key processes involved, including RNA isolation, DNase treatment, cDNA conversion, and Reverse Transcription-Polymerase Chain Reaction test (RT-PCR). These techniques decode genetic information and enhance our understanding of complex biological processes.

2.4.1 RNA extraction

After completing the transfection procedure (Section 2.2), the RNA extraction was performed using the trizol method in a fume hood under RNAse-free conditions. The excess medium from the wells was removed, and 1 mL of Trizol Reagent (Invitrogen) per condition was added. Up and down pipetting was done to ensure homogenization and aid in the lysis process. The content from the wells was transferred to 2 mL microtube

and incubated at room temperature for 5 min. Subsequently, 200 μL of chloroform (Fisher Scientific) was added, and the samples were vortexed for 15 sec, followed by a 3 min incubation at room temperature. The tubes were then centrifuged at 12,000 *x* g and 4 °C for 10 min.

After centrifugation, three distinct phases were observed: a clear and aqueous liquid on top, a cloudy and white phase in the middle, and a pink phase at the bottom. The clear phase, containing the RNA, was carefully collected into a new microtube without collecting solution from the other phases. Then, 500 μL of isopropanol (Fisher Scientific) was added, and the tube was mixed. After a 10 min incubation at room temperature, the microtube was centrifuged again under the previous conditions. The supernatant was discarded, and the resulting gel-like pellet was resuspended in 1 mL of 75% ethanol. The tube was inverted a few times and centrifuged for 5 min at 7,500 *x* g and 4 °C. This previous step was repeated, and the supernatant was again discarded. The pellet was allowed to dry for 40 min and then resuspended in 30 μL of nuclease-free H_2O. Finally, the extracted RNA was quantified using NanoDrop (Thermo Fisher Scientific) and stored at -80 °C.

2.4.2. RNA treatment with DNAse and conversion to cDNA

The preparation of DNA-free RNA samples for RT-PCR analysis was performed using the DNAse -RNAse free kit according to the manufacturer's instructions (ThermoScientific). RNA samples with a concentration of 1000 ng/μL were combined with 1 μL of 10x reaction buffer containing MgCl2. Then, 1 μL of DNAse enzyme was added, and the reaction volume was adjusted to 10 μL using DEPC-treated H_2O. The mixture was incubated at 37 °C for 30 min to degrade any remaining DNA. To stop the DNAse reaction, 1 μL of EDTA was added and incubated at 65 °C for 10 min.

To perform the cDNA synthesis, we used the cDNA Xpert kit (Grisp). Initially, in an RNAse-free microtube, 10 μL of DNA-free RNA was combined with 10 μL of 2x reaction mix. The mixture was subjected to heating at 65 °C for 5 min, followed by a 2 min incubation on ice. Subsequently, 1 μL of Xpert Rtase enzyme was added to each sample, and a brief centrifugation step was performed. The reaction was carried out under the following conditions: 25 °C for 10 min, 50 °C for 15 min, and 85 °C for 5 min. The resulting cDNA samples were either used immediately or stored at -20 °C for future applications.

2.4.3. RT-PCR

The RT-PCR samples were prepared using Xpert Fast SYBR Mix (Grisp) according to the manufacturer's instructions. Each reaction (10 μL) consisted of the following components: qPCR Master Mix (5 μL), forward primer (0.25 μL, 10 μM), reverse primer (0.25 μL, 10 μM), template DNA (2 μL, 10 ng), and RNAse-free H_2O (2.5 μL). The primers used are detailed in **Table 2.2.**

Table 2.2: RT-PCR primers sequences. 18S: 18S rRNA; F: forward; R: reverse.

Gene	Primer sequences
PIK3CA	F: 5'-GAGACATCAGCATGGCTCAA-3'
	R: 5'-TGTCCCTACCAACCAGAAGG-3'
AKT	F: 5'-CGTCCACCAAGAAGCTGAG-3'
	R: 5'- GCCGTCAGAAAACATGTCAG-3'
MTOR	F: 5'- AGCCTGGGTCAAAGAAGTCA-3'
	R: 5'- GCCAACCCTCCTTCACAATA-3'
18S	F: 5'-AAACGGCTACCACATCCAAG-3'
	R: 5'-CCTCCAATGGATCCTCGTTA-3'

For the reaction setup, the DNA template was pipetted onto qPCR plates, followed by the addition of the primer mix (8 μL/well). The qPCR plate was sealed and subjected to thermal cycling using the RT-PCR System. The reaction conditions involved an initial step at 95 °C for 3 min, followed by 39 cycles of 95 °C for 3 sec, 60 °C for 30 sec, and a final extension at 65 °C for 5 min. In this context, **Figure 2.2** is a simplified visual representation of the protocol.

Ct values were obtained using the Bio-Rad CFX Manager Software, and relative expression levels were determined using the 2-ΔCt method, according to the formula: ΔCt (target gene) = Ct (target gene)-Ct (control gene) [101], with the 18S gene as the housekeeping gene.

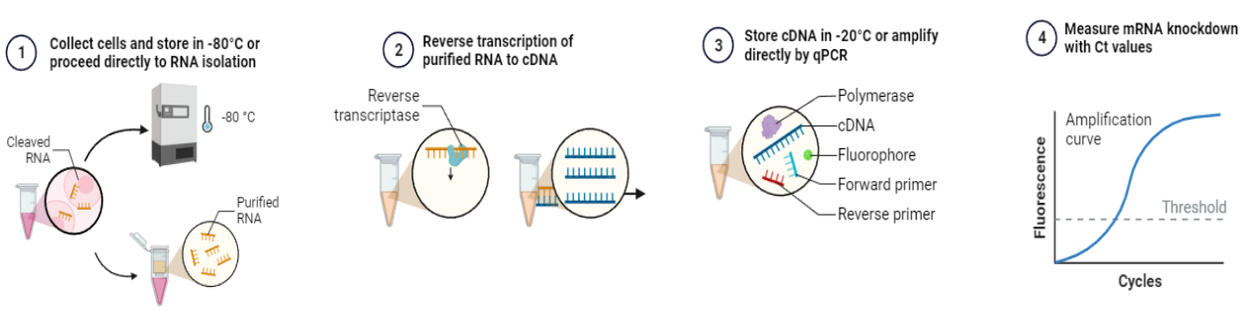

Figure 2.2: Schematic representation of the Reverse transcription polymerase chain reaction procedure including treatment with DNAse, conversion to complementary DNA and relative expression levels analysis. qPCR: quantitative polymerase chain reaction, CT: cycle threshold. Created with BioRender.

2.5 Cell viability assessment

The *in vitro* toxicity was determined by 3-(4,5-dimethylthiazol-2-yl)-2,5-diphenyltetrazolium bromide (MTT) (Sigma-Aldrich) assay. The reduction of MTT from yellow tetrazolium die to purple crystals is the foundation for this colourimetric assay. By using a spectrophotometric analysis after dimethyl sulfoxide (DMSO, Sigma-Aldrich), it is possible to determine the viability of the cells.

According to section 2.2, the transfection procedure was executed in 96-well plates. After the transfection period was over, the medium was removed and 100 µL of MTT (0.5 mg/mL) was added to each well. To dissolve the MTT crystals, 100 µL of DMSO was added to each well after 2 h of incubation. This solution was then left at room temperature for 10 min. The plate was then agitated, and the cell viability was assessed using a microplate reader (Cytation 3, BioTek) to measure absorbance at 570 nm.

2.6 Evaluation of Cellular Migration Ability

The scratch assay is an *in vitro* technique that allows a comprehensive evaluation of the effects of siRNA on cellular migration over time, providing valuable insights into the therapeutic potential of the treatment.

After conducting the cellular transfection procedure as described in Section 2.2, a controlled scratch wound was created across the surface of a 6-well plate using a large 1000 µL pipette tip. The plates were then incubated under optimal conditions at 37 °C with 5% CO_2.

Microscopic images of the scratch wounds were captured at designated time intervals, including 0 h, 3 h, 6 h, and 24 h post-transfection. The wound areas were quantified using ImageJ software, enabling a comparative analysis of changes in wound size across different conditions and time points.

The percentage of wound recovery was calculated by comparing the gap area at each time point with the initial gap area recorded at 0 h.

2.7 Exosome isolation and characterization

The isolation procedure for exosomes followed established protocols by our laboratory [88]. Briefly, cells were cultured in T175 flasks under specified conditions until they reached 80% confluency. The culture media was then removed, and the flasks were washed with 3 mL of PBS 1x. Subsequently, 15 mL of serum-

free DMEM was added. After 48 h, the media was collected in falcon tubes and subjected to two consecutive centrifugation steps at 800 *x* g for 5 min and 2,000 *x* g for 10 min. The supernatant was then filtered using 0.2 µm into new 50 mL falcon tubes. Subsequently, the samples were ultracentrifuged at 100,000 *x* g for 3 h at 4 °C. The resulting exosome pellets were resuspended in 50 µL of sterile PBS 1x, transferred to a microtube, and stored at -80°C, as illustrated in **Figure 2.3.**

To determine the concentration and size of the isolated exosomes, we used Nanoparticle Tracking Analysis (NTA). This technique allows for the measurement of single particle concentration and size as they are illuminated and recorded in a video. To prepare the exosome samples for NTA, they were diluted at a 1:5 ratio with PBS 1x. Subsequently, the diluted samples were collected and analyzed using the NanoSight (Nanosight, Salisbury) equipment. For each sample, two 60 sec videos were recorded, with a 25 ms camera shutter, while the equipment adjusted its focus to capture the nanoparticles effectively. The NanosSight program provided essential data, including mean, mode, and particle concentration of the HEK-derived exosomes, which was extracted using Nanoparticle Tracking Analysis Version 2.3 software.

To further analyze exosome size and zeta potential, we turned to Dynamic Light Scattering (DLS). The exosome samples were diluted at a 1:10 ratio with PBS 1x and subsequently loaded into the appropriate cuvettes. The size and zeta potential measurements were then calculated using Zetasizer (Malvern Panalytical). For zeta potential measurements, we conducted 12 runs per sample. To obtain size measurements, each sample was measured with a camera level set at 5.5 mm, and triplicate measurements were taken for each biological sample. Subsequently, the data was analyzed using Zetasizer Nano software 3.3.

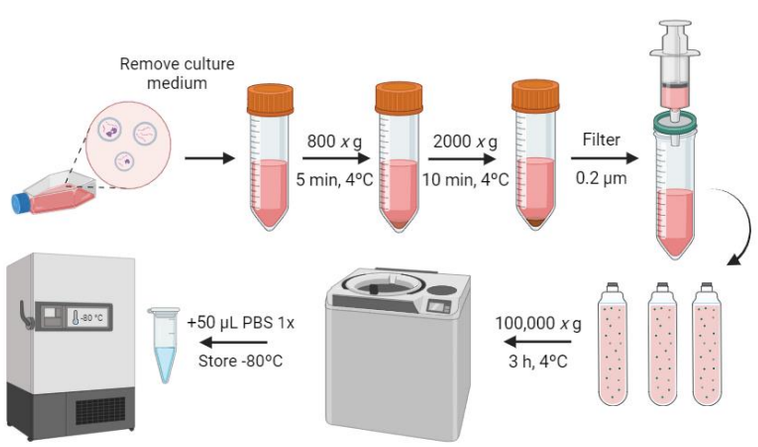

Figure 2.3: Schematic representation of the isolation procedure for exosomes [88]. Created with BioRender.com

2.8 siRNA loading into Exosomes via electroporation.

Our laboratory has developed and refined an electroporation protocol to efficiently load siRNA molecules into exosomes isolated from cells [88]. The process begins with the preparation of an electroporation buffer under sterile conditions. This buffer is composed of 19.2 μL of 3M K2HPO4, 417 μL of 3M KCl, and 10.5 mL of Opti-Prep (StemCell Technologies), with PBS 1x added to achieve a final volume of 50 mL. This buffer, once prepared, can be stored for up to six months at a temperature of 4°C, ensuring its long-term utility.

Subsequently, the siPIK3CA is combined with HEK-Exo at a precise ratio of 1:2 (siRNA: exosomes, in μg:μg), and this mixture is further supplemented with 400 μL of the previously prepared electroporation buffer. The resulting solution is loaded into specially designed electroporation cuvettes, where the electroporation process takes place.

Electroporation was carried out at controlled parameters of 400 V and 125 μF capacitance for a duration of 10 s for each condition. This optimized electroporation protocol ensures the efficient loading of siPIK3CA into the exosomes, leading to the formation of siRNA-loaded exosomes, referred to as Exos-siPIK3CA.

To purify and isolate the Exos-siPIK3CA, ultracentrifugation is employed at 180,000 *x* g for 2 h at a temperature of 4 °C. This step effectively separates the electroporated exosomes from unwanted components, and the resulting supernatant is carefully aspirated. The Exos-siPIK3CA, now enriched with the siPIK3CA cargo, are then resuspended in an appropriate volume of DMEM, tailored to meet the specific requirements of subsequent transfection experiments.

2.9 Cellular assays with siRNA-loaded exosomes

The Exos-siPIK3CA were transfected onto the previously selected cell lines. RKO and HCT-15 were initially seeded in a 6-well tissue culture plate at a density of 3.0 x 10^5 cells per well, 24 h prior to transfection. The following day, when cells reached a confluence of 50-70%, the culture medium was replaced with 750 μL of serum-free DMEM. Exos-siPIK3CA solution was prepared separately and added to each well, and cells were incubated for 6 h, 24 h and 48 h at different time points.

For transfections using 96-well plates, 200 μL of complete medium with 1.0 x 10^4 cells per well was

added. Cells were then incubated overnight at 37 °C with 5% CO_2. On the next day, the Exos-siPIK3CA mix was added to the corresponding wells and cells were incubated for transfection for specified time points 6 h, 24 h, and 48 h.

To comprehensively evaluate the effects of Exos-siPIK3CAs, a battery of assays was executed, including Western Blot (section 2.3), RT-PCR (section 2.4), and MTT (section 2.5).

2.9.1 Cell migration assessment of siRNA-loaded exosomes

Following section 2.2, this assay was instrumental in evaluating the proliferation and cell migration effect with Exos-siPIK3CA.

A controlled scratch wound was created in a 6-well plate, followed by incubation at 37 °C with 5% CO_2. Images at 0 h, 6 h, and 24 h post-transfection were analyzed using ImageJ software to quantify wound areas. The wound recovery percentage was calculated by comparing gap areas at each time point with the initial gap at 0 h.

2.10 Statistical Evaluation

The analysis of results obtained from various experiments was conducted utilizing GraphPad Prism 8 Software, developed by Graphpad Holdings. To ascertain statistical significance across all data, a two-way analysis of variance (ANOVA) was employed, complemented by the Sidak's multiple comparisons test. In the context of this analysis, a p-value (p) <0.05 was indicative of the existence of statistically significant differences between the experimental groups.

3. Results and Discussion

3.1 Assessment of cell growth and viability after siPIK3CA treatment

The transfection method was conducted using the Lipofectamine RNAi-Max reagent. The siPIK3CA was transfected onto the HCT-15 and RKO cell lines. This reagent is a lipid-based carrier system that facilitates the cellular uptake of siRNA by forming lipoplexes with anionic acids. These complexes navigate to the cell membranes via endocytosis, and intracellularly, the siRNA dissociates from the complex and selectively binds to the target gene *PIK3CA* [102]. This technique enabled the analysis of the gene function, and the effect was evaluated through MTT, Western Blot and RT-PCR of the PAM pathway.

It is important to note that, in our research, we used specific CRC cell lines, HCT-15 and RKO. These CRC cells bear distinct mutations within the *PIK3CA* gene, which are frequently located near specific regions: E545K (exon 9), as observed in HCT-15 cells, and H1047R (exon 20), as identified in RKO cells.

Zhao L *et al.* [103] demonstrated that mutations in *PIK3CA* result in the hyperactivation of the PAM pathway which then transforms PIP2 into PIP3. High levels of PIP3 lead to phosphorylation of Akt, which showed an impact on the cancer cell cycling, survival and growth. Remarkably, Wang *et al.* [104] demonstrated a higher frequency of mTOR gene expression in *PIK3CA* mutant patients compared to wild-type patients, suggesting the potential for differential sensitivity to PAM pathway inhibitors.

These mutations serve as pivotal focal points in our ongoing investigation into gene and protein expression dynamics. This is crucial as we aim to discern variations in cellular behaviour across different assays.

The cellular viability of the two cell lines was assessed using an MTT assay at 24 h, 48 h and 72 h post-transfection using Lipofectamine with siPIK3CA **(Figure 3.1)**, testing two different final concentrations of siRNA, 25 nM and 50 nM. Additionally, we also conducted this assay at later time points, specifically at 96 h and 120 h **(Figure A.2 in Supplementary Information)**, to gain a more comprehensive understanding of the long-term impact of the treatment on cellular viability. To ensure the integrity of our analysis, non-treated cells were included as our control group. Additionally, cells treated solely with Lipofectamine were examined to discern the influence of this reagent on our results.

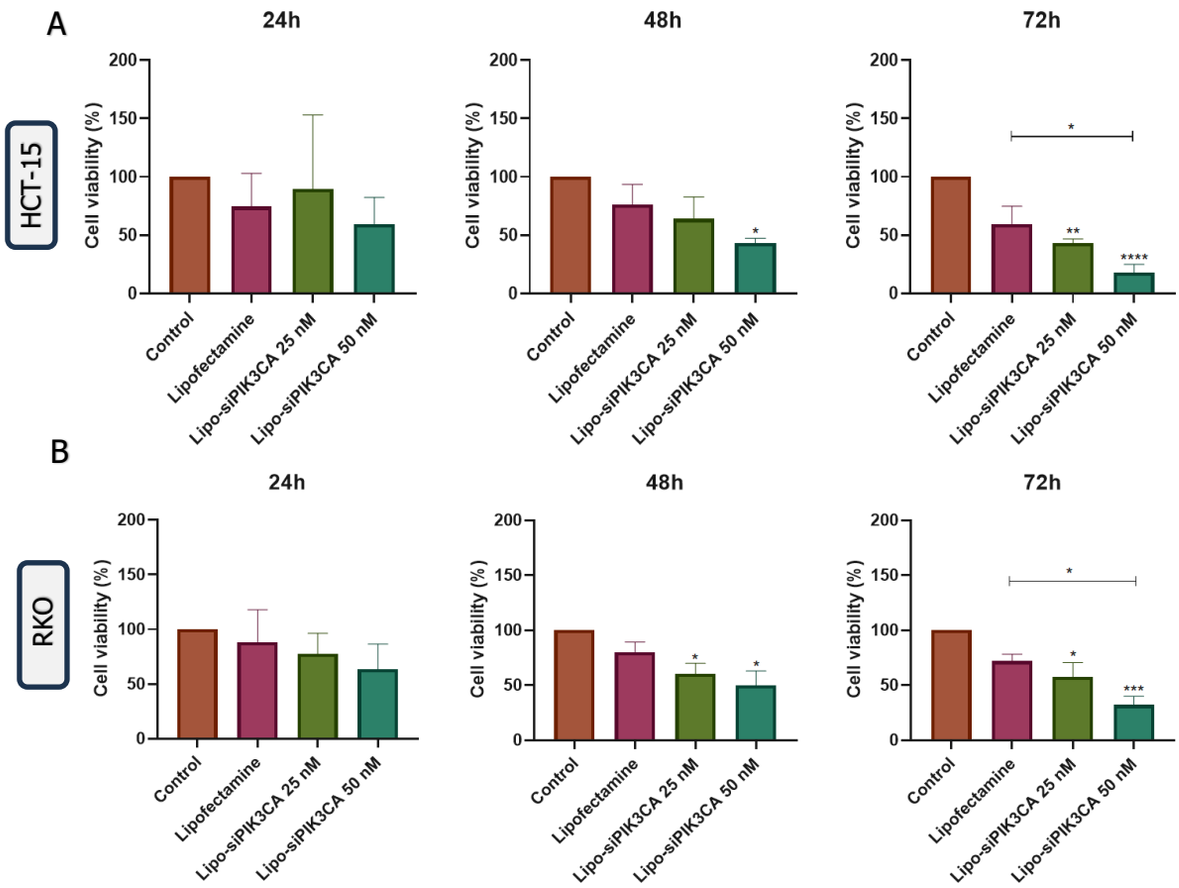

Figure 3.1: Assessment of the cellular viability promoted by siPIK3CA: Evaluation of **(A)** HCT-15 and **(B)** RKO cellular viability treated with Lipofectamine and *siPIK3CA* (25 nM or 50 nM) over 24 h, 48 h and 72 h. For each time point, viability was estimated by the MTT assay. All data is presented as the percentage of cell viability ± SD of three independent experiments. Two-way ANOVA indicates statistically significant differences within the group assessed by Sidak's post-test and denoted as follows: non-significant $p > 0.05$, *$p \leq 0.05$, **$p \leq 0.01$, ***$p \leq 0.001$ and ****$p \leq 0.0001$.

In both cell lines, there are no statistical differences between the control group and only lipo-transfected cells ($p > 0.05$). Having that said, although we see a statistical difference for the two different cell lines, with Lipo-siPIK3CA 50 nM, at 48 h in comparison with the control group, the same does not apply between the Lipo-transfected cells.

In both cell lines, the most substantial decrease in cellular viability was observed when using 50 nM siRNA, resulting in a cell reduction to 17.8% ± 4.9% for HCT-15 ($p \leq 0.0001$), and 32.1% ± 3.8% for RKO ($p \leq 0.001$) cells after 72 h. Importantly, this is the only time point and condition which exhibited statistical significance when compared to both the control group and the Lipofectamine-only treatment. These results are consistent with the findings reported by Silva *et al.* [88]. In their transfection study, the researchers utilized Lipofectamine along with siRNA-targeting *PIK3CA* on MDA-MB-231 and MDA-MB-453 cell lines, achieving a similar conclusion. They concluded that the most significant reduction in cellular viability was reached when assessing the 72 h time point and using the highest siRNA final concentration of 50 nM. Furthermore, Vaidya

et al. [105] demonstrated the challenges associated with the efficiency of naked siRNA by revealing a 30% reduction in cellular viability when siRNA was used in conjunction with Lipofectamine.

Our MTT results indicate that the survival rate of cells remains at 20-30% for the highest concentration and longer incubation time of 72 h, showing the elevated significance of the results for the Lipo-siPIK3CA effect on cellular viability. Comparing the results obtained at 96 h and 120 h for RKO cells, **(Figure A.2 in Supplementary Information)**, we did not observe a greater decrease in cell viability, which maintained approximately 25%. Furthermore, we did not achieve relative significance ($p > 0.05$) in relation to the lipofectamine control.

Since there was only one time point where we obtained statistical significance for all parameters, we decided to proceed with the study using the 72 h time point and 50 nM siRNA.

3.2 Evaluation of Gene and Protein Expression after siPIK3CA

Gene and Protein expression are fundamental biological processes, where the genetic instructions stored in DNA are translated. In this investigation, we focus on understanding the complexities of both expressions, specifically examining the impact of Lipo-siPIK3CA on the PI3K/Akt/mTOR pathway **(Figure 3.2 A)**. To pursue such goals, we employed Western blot and RT-PCR analysis, which allowed us to explore the interplay between PI3K, Akt and mTOR expression.

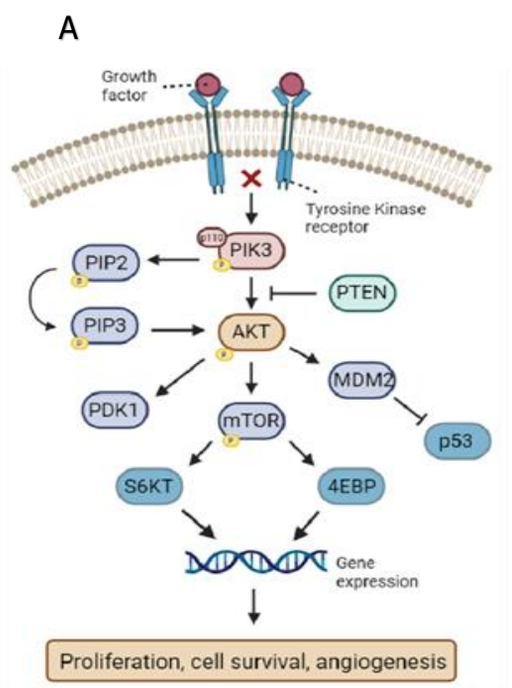

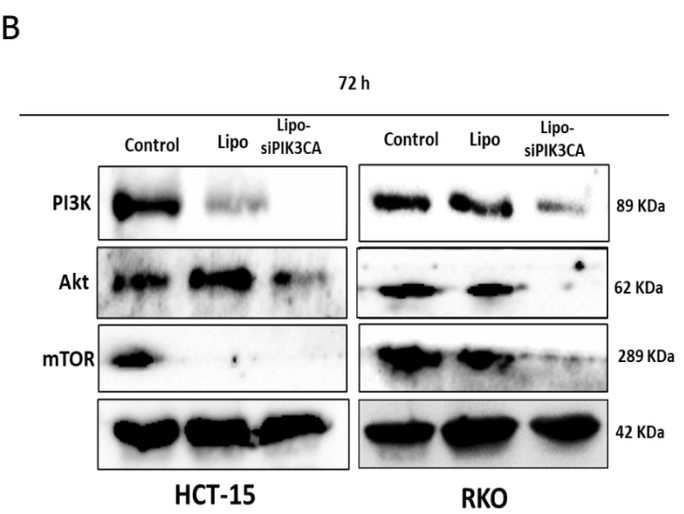

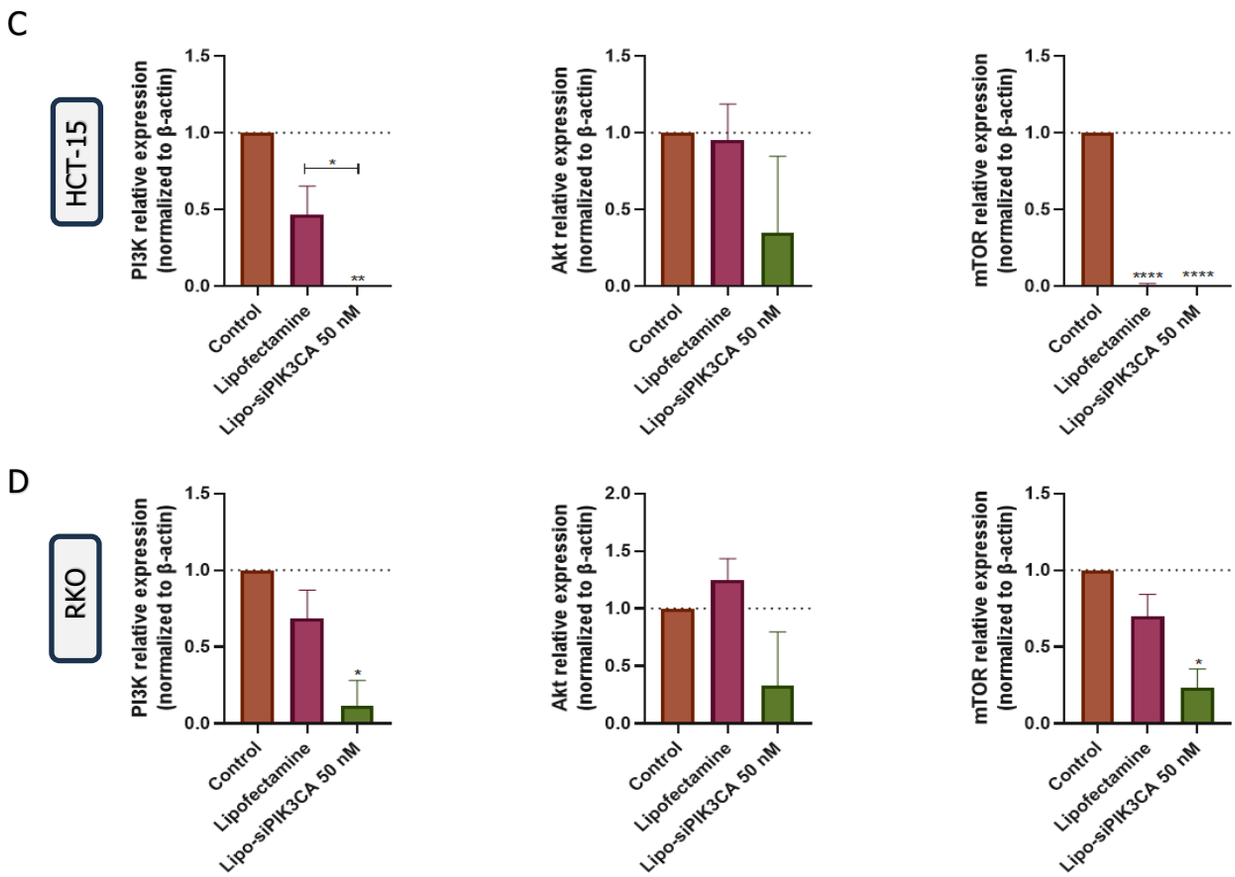

Figure 3.2: Impact of siPIK3CA transfection with Lipofectamine on PI3K/Akt/mTOR Pathway through Western Blot: In **(A)**, a simplified illustration of the PAM pathway. This crucial signaling cascade is initiated by various stimuli, including growth factors, which recruit PI3K, leading to the conversion of membrane-bound PIP2 to PIP3. Subsequently, AKT and PDK1 are activated through binding to PIP3. PTEN regulates AKT by dephosphorylating PIP3. AKT influences cell growth by affecting the MDM2 complex and mTORC signaling. Activation of the complex leads to the formation of mTORC1, which, in turn, triggers cell growth, proliferation and angiogenesis by S6KT and 4EBP. Key components include phosphatidylinositol 3-kinase (PI3K), protein kinase B (AKT), 3-phosphoinositol-dependent protein kinase-1 (PDK1), phosphatase and tensin homolog (PTEN), phosphatidylinositol 4,5-bisphosphate (PIP2), phosphatidylinositol (3,4,5) trisphosphate (PIP3), mechanistic target of rapamycin (mTOR), ribosomal protein S6 kinase T (S6KT), 4E-binding protein (4EBP). Created with BioRender.com
(B): Evaluation of protein expression level in HCT-15 and RKO cells through Western Blot. Assessment of Lipo-siPIK3CA transfection of PI3K, Akt, mTOR and β-actin proteins treated with siPIK3CA (50 nM) for 72 h. Relative quantification of PI3K, Akt, and mTOR protein levels in HCT-15 **(C)** and, RKO **(D)** cells, post Lipo-siPIK3CA transfection with *siPIK3CA* (50 nM) for 72 h. These results show the fold change, representing two independent experiments. The fold change is calculated concerning the control group and was normalized to the reference protein, β-actin. Two-way ANOVA indicates statistically significant differences within the group assessed by Sidak's post-test and denoted as follows: non-significant $p > 0.05$, *$p \leq 0.05$, **$p \leq 0.01$ and ****$p \leq 0.0001$.

In HCT-15 cells, our Western blot analysis **(Figure 3.2 B** and **C)** revealed a significant reduction, reaching 0.4 ± 0.1-fold in PI3K protein levels when treated with Lipofectamine, and a complete absence of PI3K protein expression, presenting null values, in response to Lipo-siPIK3CA 50 nM, compared to the control group ($p \leq 0.01$). Interestingly, Akt expression in HCT-15 cells remained relatively the same in the Lipofectamine group. However, when subjected to Lipo-siPIK3CA 50 nM treatment, we observed a reduction to approximately 0.3-fold in Akt protein expression although we did not see any statistical significance ($p > 0.05$). Furthermore, mTOR expression in HCT-15 cells exhibited also a reduction to PI3K, with a significant

reduction, approaching near-null values, in response to Lipofectamine and Lipo-siPIK3CA 50 nM treatment.

Turning our attention to RKO cells **(Figure 3.2 B** and **D)**, we observed similar dynamics in response to the experimental conditions. Lipo-siPIK3CA 50 nM treatment led to a reduction of approximately 0.2 ± 0.2-fold in PI3K expression in RKO cells. It is noteworthy to mention that the results obtained in the Akt protein expression analysis for RKO cells closely mirrored those of the HCT-15 cells. Interestingly, mTOR expression in RKO cells exhibited a significant reduction of approximately 0.3 ± 0.2-fold when treated with Lipo-siPIK3CA. Moreover, the consistent reduction in mTOR expression in both HCT-15 and RKO cells suggests a possible convergence of regulatory mechanisms influencing mTOR activity in these two cell lines. A study conducted by Weigelt *et al.* [106] reported that cancer cells with activated *PIK3CA* mutations respond differently to mTOR inhibitors compared to cells that lack such mutations.

Silva *et al.* [88] results also showed a significant decrease in PI3K protein levels in TNBC cell lines, reaching a maximum decrease in PI3K protein expression of 0.2 ± 0.1-fold, after 72 h transfection with Lipofectamine and siRNA targeting *PIK3CA*.

On the other hand, while we successfully reduced PI3K and mTOR protein levels, we did not see the same effect on Akt ($p > 0.05$). *In vitro* experiments by Dufour *et al* [107] showed that the anti-proliferative effects of PI3K inhibitors are enforced by Akt inhibitors by only transiently blocking Akt signaling. Although, Akt serves as a critical connection between mTORC1 and mTORC2 after PI3K activation [22,23]. It is possible that when we knocked down PI3K and mTOR, it mostly affected downstream signals without directly changing Akt levels. Akt activity may still be maintained through alternative signaling pathways or compensatory mechanisms, such as the MAPK/ERK pathway or NF-κB pathway [107], contributing to the observed stability in Akt levels.

At the protein level, Western blot analysis **(Figure 3.2 B, C** and **D)** confirmed the reduction of PI3K and mTOR levels over 72 h time-point, indicating the effectiveness of siPIK3CA treatment in these CRC cells.

Our RT-PCR analysis explored *PI3K* and *mTOR* expression dynamics, **(Figure 3.3 A** and **B).**

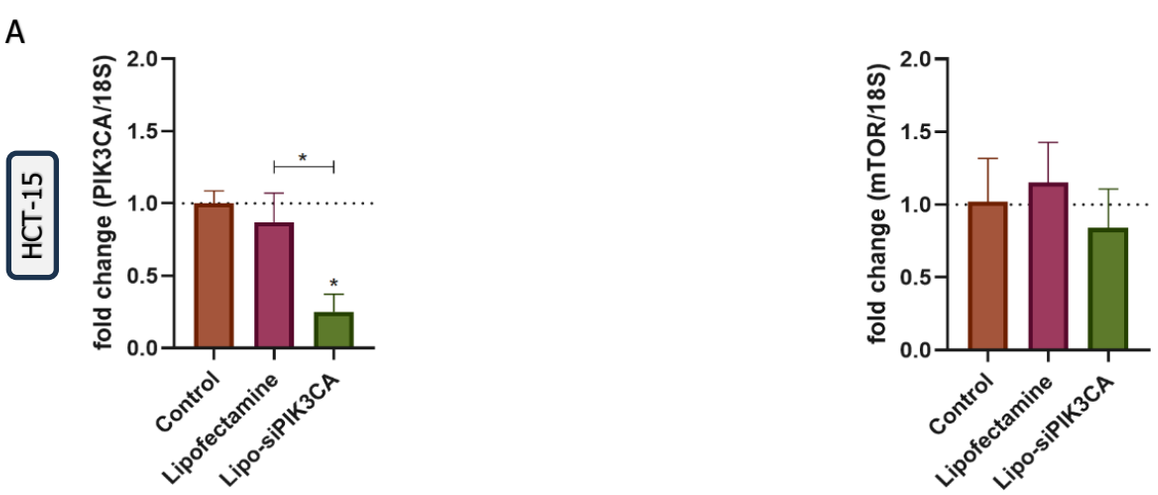

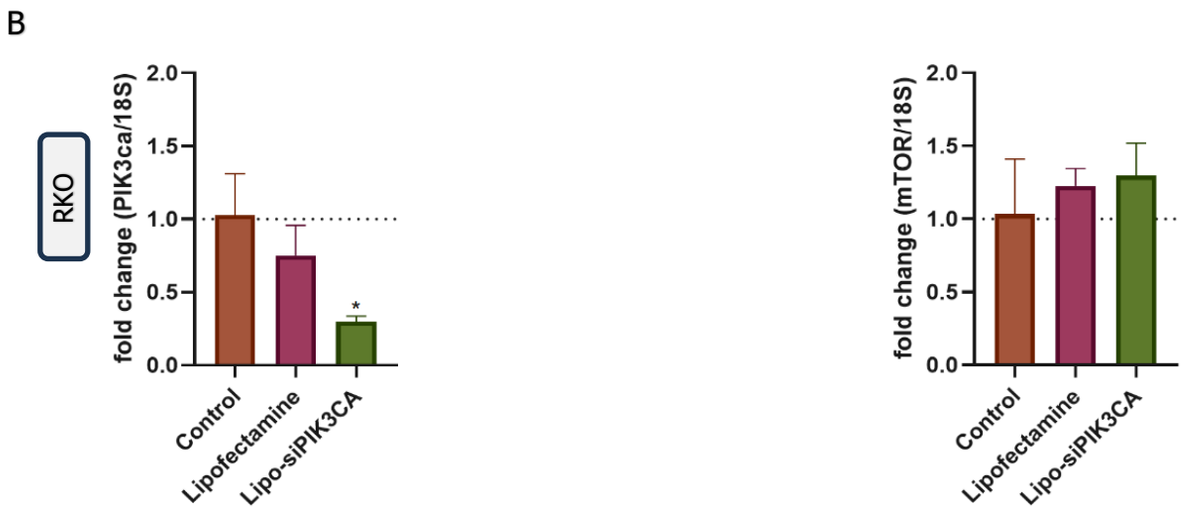

Figure 3.3 Assessment of gene silencing expression of *PIK3CA* and *MTOR*: Relative quantification of mRNA levels in both **(A)** HCT-15 and **(B)** RKO cells post Lipo-siPIK3CA transfection with siPIK3C*A* (50nM) after 72 h. These results show the fold change, representing two independent experiments. The fold change is calculated concerning the control group and was normalized to the reference gene, 18S rRNA. Two-way ANOVA indicates statistically significant differences within the group assessed by Sidak's post-test and denoted as follows: non-significant $p > 0.05$ and $*p \leq 0.05$.

Regarding *PIK3CA* expression, upon transfection with Lipofectamine condition, we did not observe significant responses ($p > 0.05$) in *PIK3CA* expression for both cell lines. The most notable effect occurred under the influence of Lipo-siPIK3CA, where HCT-15 cells experienced a profound drop of approximately 84% in *PIK3CA* expression. In RKO cells, a similar trend emerged with a substantial reduction of about 78% gene expression. Although there was a further decrease in *PIK3CA* expression of HCT-15 cells, both showed statistical significance ($p \leq 0.05$).

Moving on to *AKT* gene expression, we faced a challenge during our analysis. Despite our best efforts, we were unable to achieve any amplification of *AKT* gene expression in either HCT-15 or RKO cells across all treatment conditions. This unexpected outcome was attributed to issues with the primers used in our experiments, which warrants further investigation to ensure the reliability of future results in this regard.

In the domain of *MTOR* expression **(Figure 3.2 A** and **B)**, HCT-15 and RKO cells under Lipofectamine and Lipo-siPIK3CA treatment, displayed a relatively consistent response, showing no significant differences ($p > 0.05$).

Overall, while both cell lines exhibited a reduction in *PIK3CA* expression when exposed to Lipo-siPIK3CA 50 nM, the extent of this reduction varied. HCT-15 demonstrated a more pronounced response, being the only one to show statistically significant differences between the control and Lipofectamine groups.

This discrepancy suggests the influence of nuanced regulatory mechanisms, possibly attributed to distinct mutation profiles in different cellular contexts [28,29]. HCT-15 cells bear the E545K and KRAS mutation, while RKO cells carry the H1047R mutation and KRAS wild-type. Valentino *et al* [108] reported that when

they combined *PIK3CA + KRAS* treatments, the expression of *PIK3CA* gene was reduced in HCT-116 (which have the same exact mutation site of RKO) and DLD1 cells (with the same exact mutation site of HCT-15). Additionally, the researchers revealed that the sensitivity to siRNA treatments are influenced by the mutational status of cancer as evidenced by the reduced response to treatments targeting pathways in CRC cells in which the mutant allele had been removed.

Silva *et al.* [88] obtained comparable findings, observing a more significant downregulation of *PIK3CA gene* expression with the same Lipo-siPI3KCA treatment in the TNBC cell lines, mirroring our own results.

Overall, analyzing the results from the Western Blot and RT-PCR, Lipo-siPIK3CA successfully targets the *PIK3CA* gene in both cells. First, Lipo-siPIK3CA promotes both a *PI3K* protein and gene knockdown, as observed by Western Blot and RT-PCR, for both cell lines. Akt maintained levels similar to those of the control group. On the other hand, a noticeable decrease in mTOR protein expression was observed, suggesting a potential convergence of regulatory mechanisms influencing mTOR activity in these two cell lines [104,106]. These results end up disagreeing with the RT-PCR results when Lipo-siPIK3CA does not induce the decrease of mRNA expression of *MTOR*. This discrepancy in levels underscores the role of post-transcriptional regulatory mechanisms in protein expression. These mechanisms, which may include phosphorylation and ubiquitination, which tend to decrease the protein level, can independently influence protein stability and translation from mRNA expression [104,106,109].

Since the lipofectamine-only condition did not promote significant effects on cells ($p > 0.05$), with the exception of mTOR relative expression in HCT-15, it is possible to conclude that the effect observed is not stimulated by lipofectamine, but only by the siPIK3CA action. Furthermore, RT-PCR and Western Blot analysis indicate that HCT-15 cells are more susceptible to Lipo-siPIK3CA treatment, which can be associated with the different *PIK3CA* mutations.

3.3 Isolation and characterization of exosomes derived from the HEK-293t cells

Exosomes were isolated from the non-tumorigenic HEK-293t cells to ensure the absence of potentially carcinogenic materials from the parental cells [110], following the previously documented extraction protocol (Section 2.7). Following differential centrifugation isolation, these exosomes were characterized, assessing their size, mean, mode, zeta potential, PDI, and the presence of exosome surface protein markers **(Figure 3.4)**.

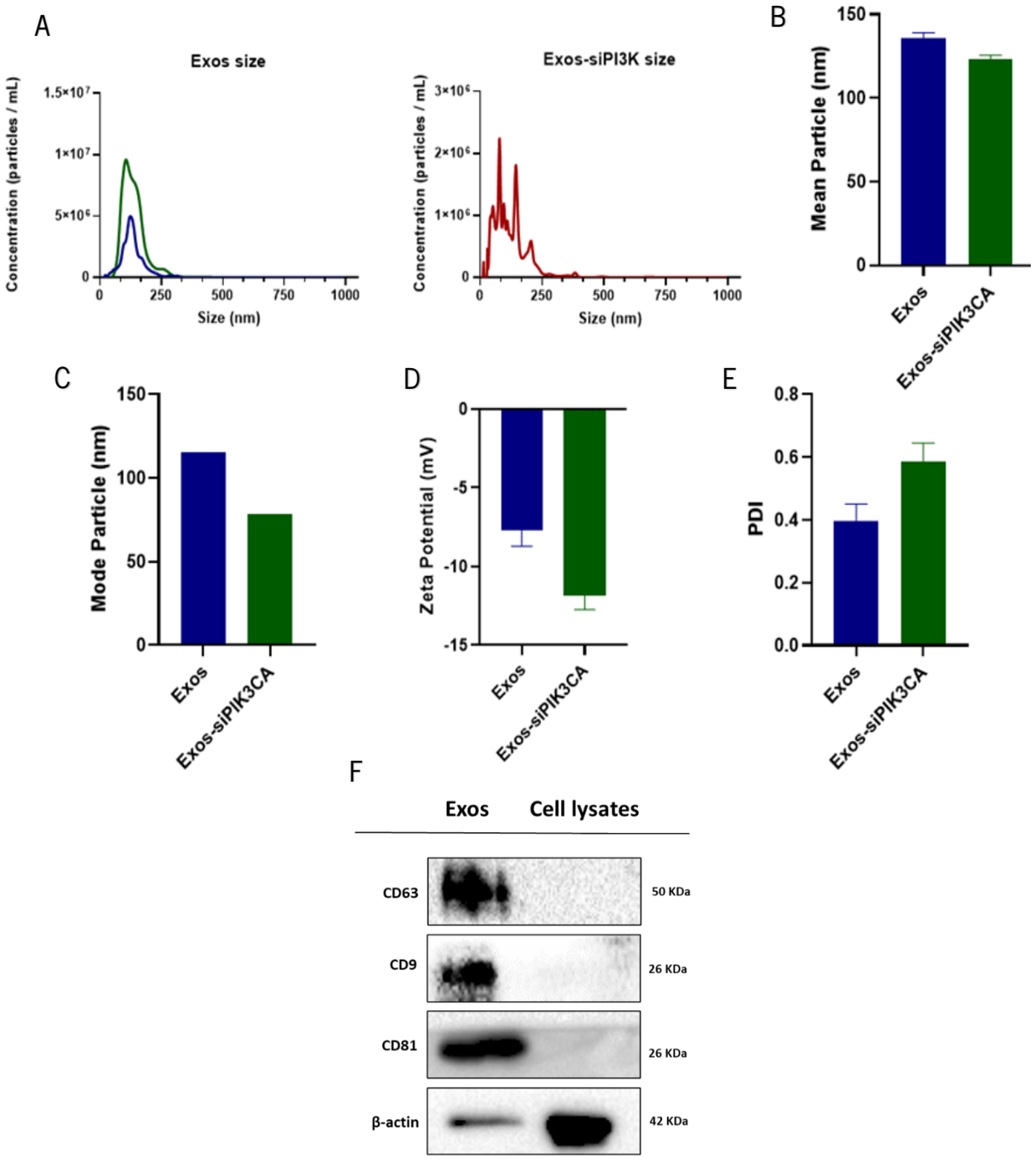

Figure 3.4: Isolation and characterization of exosomes derived from the HEK-293t cells. Characterization of HEK-293t exosomes and Exos-siPIK3CA in terms of **(A)** Concentration (particles/mL) and size distribution (nm), **(B)** Mean particle diameter (nm), **(C)** Mode particle diameter (nm), **(D)** Zeta potential (mV) and **(E)** Polydispersity index (PDI). **(F)** Western blot for exosome markers CD9, CD63, CD81, Alix and exclusion marker β-actin. HEK cell lysate; HEK Exosomes. Data is representative of one independent experiment. Two-way ANOVA indicates statistically significant differences within the group assessed by Sidak's post-test and denoted as follows: non-significant $p > 0.05$ and $*p \leq 0.05$.

The analysis revealed average diameters of 134 nm (Exos 1 e 2), and 122 nm (Exos-siPIK3CA) using NP tracking analysis **(Figure 3.4 A, B** and **C).** For example, in Théry. C *et al* [111], EVs are classified as exosomes only if they fall within the 30-150 nm range. For instance, Ferreira *et al.* [112] reported a mode of

approximately 110 nm for human fibroblast (BJ) cell-derived exosomes, while Mendt *et al.* [113] noted an approximate size of 100 nm. Notably, we also detected populations of vesicles exceeding 200 nm, which may represent other vesicles within the sample or aggregates formed during the isolation process, suggesting a heterogeneous population, a recognized challenge in exosome research [114].

Furthermore, we assessed zeta potential and PDI, **(Figure 3.4 D** and **E)** using DLS. A significant decrease of zeta potential was observed for Exos-siPIK3CA (-11.83 mV) compared to only exosomes (-7.4 mV), attributable to the negatively charged siRNA content, consistent with the results found by Didiot MC *et al.* [114], when incorporating siRNA within U87-derived exosomes and Ferreira *et al.* [112] when incorporating siRNA for BJ-derived exosomes. Similarly, a slight increase in PDI was observed in Exos-siPIK3CA, becoming slightly more heterogeneous or varied. This result is consistent with the characteristics documented in [116].

Western blot analysis revealed the presence of the tetraspanins, CD9, CD63, and CD81 commonly expressed on the surface of the exosomes, as observed in HEK-Exos **(Figure 3.4 G).** Notably, the commonly used exclusion marker, β-actin [117], was detected in both HEK lysates and our exosomes, raising questions about the purity of our exosome preparation. This result may be related to the high PDI, where we obtained some particles above 200 nm, potentially indicating that some of these particles may not be exclusively exosomes [114]. To solve this problem, it would be necessary to optimize the centrifugation part of the protocol or add an additional purification step.

In summary, our exosomes were successfully isolated and characterized, resulting in exosomes with appropriate size, mean, mode, zeta potential, and PDI, along with the presence of exosome surface markers in our Exos-siPIK3CA.

3.4 Exploring the Potential of Exosome-Mediated siPI3KCA Delivery

In the world of medical innovation, the success of siRNA-based therapy relies on effectively delivering siRNA to the intended tumor cells. This is essential to protect these cells from natural challenges, such as enzymatic breakdown, and to promote uptake into the cells. Once inside, siRNA can operate within the cell's cytoplasm and engage with the target [73,74,75]. The second part of our study begins with a crucial step: validating *in vitro* loading of siPIK3CA within Exosomes. They serve the dual purpose of shielding siRNA from degradation and enhancing its uptake into target cells. Through the use of exosomes, our aim is to maximize the effectiveness of siPIK3CA on the specific CRC cells we are targeting.

The following analysis **(Figure 3.5)** examines the changes in HCT-15 and RKO cells in response to Exos-siPIK3CA treatment, highlighting significant shifts in protein expression in the PAM pathway.

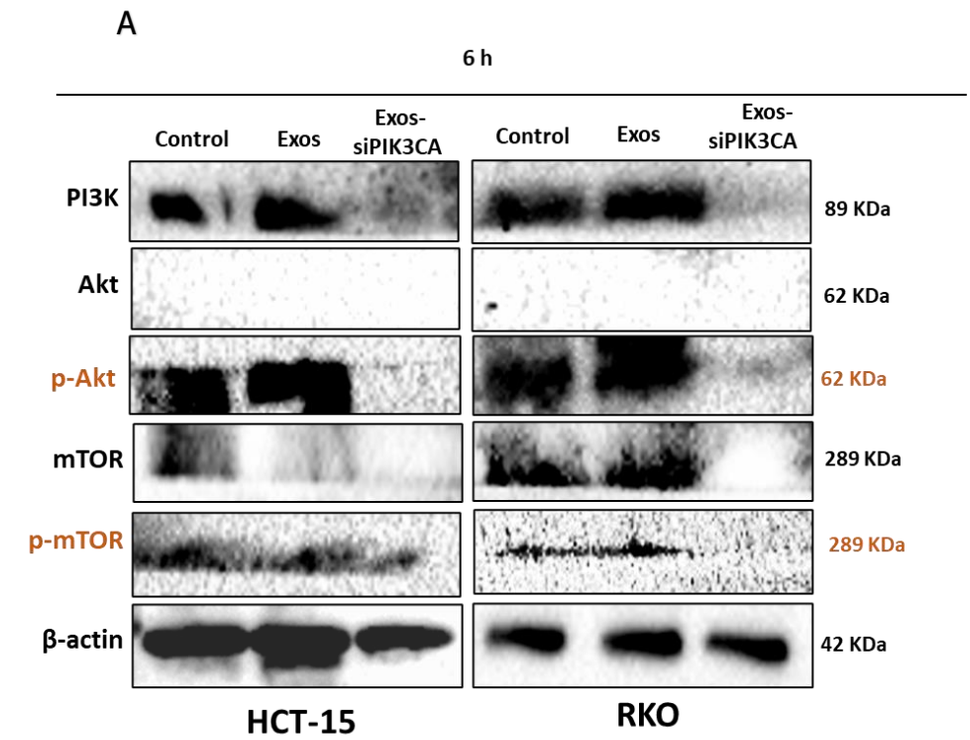
A
6 h
Control
Exos
Exos-siPIK3CA
Control
Exos
Exos-siPIK3CA
PI3K
89 KDa
Akt
62 KDa
p-Akt
62 KDa
mTOR
289 KDa
p-mTOR
289 KDa
β-actin
42 KDa
HCT-15
RKO

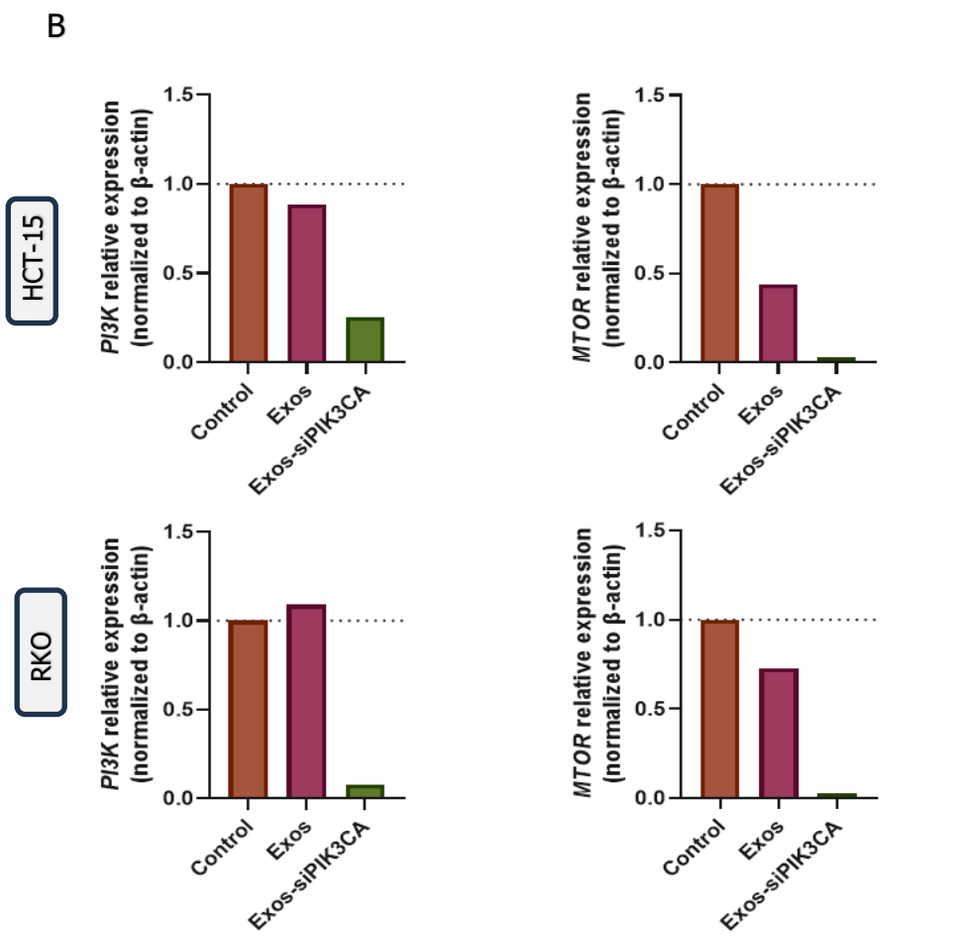
B
HCT-15
RKO
PI3K relative expression (normalized to β-actin)
MTOR relative expression (normalized to β-actin)
1.5
1.0
0.5
0.0
Control
Exos
Exos-siPIK3CA

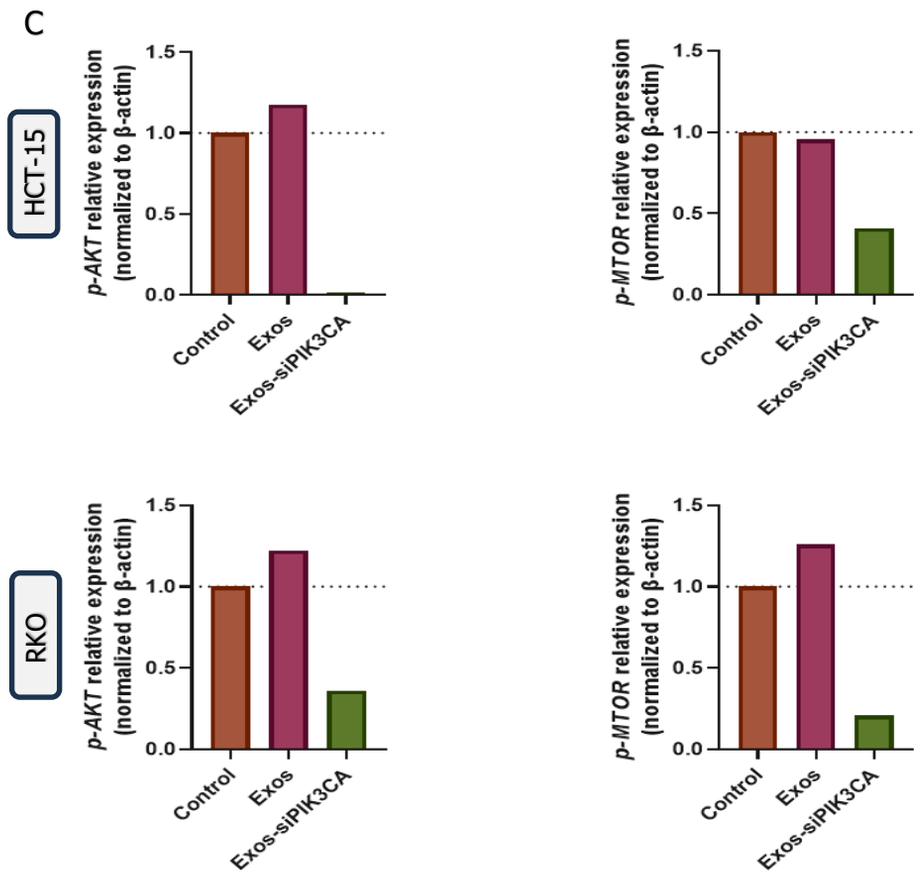

Figure 3.5: Evaluation of siPIK3CA Electroporation with Exosomes on PI3K/Akt/mTOR Pathway through Western Blot: (A) Western Blot of Exos-siPIK3CA transfection of PI3K, Akt, p-Akt, mTOR, p-mTOR and β-actin treated with siPIK3CA (50 nM) for 6 h. **(B)** and **(C)** Represent the relative quantification of **(A)** protein levels in HCT-15 and RKO cells post Exos-siPIK3CA electroporation with siPIK3CA (50 nM) for 6 h. Data is representative of one independent assay.

To ensure the integrity of our analysis, non-treated cells were included as our control group and cells treated solely with exosomes were examined to discern the influence of these particles on our study.

In HCT-15 cells, our Western Blot analysis **(Figure 3.5 A** and **B)** revealed in Exos-siPIK3CA treatment, a substantial reduction in PI3K protein expression to 0.2-fold. Unfortunately, no bands were observed in Akt, suggesting that there were some issues associated with the Western Blot protocol. When treated with Exosomes (Exos), there was a significant reduction in mTOR protein expression to 0.5-fold. On the other hand, when combined with siPIK3CA treatment, there was a further reduction indicating a near-null decrease in mTOR protein expression.

Regarding the phosphorylated Akt and mTOR **(Figure 3.5 A** and **C),** in HCT-15 cells, when treated with Exos, there was a slight increase in p-Akt expression (approximately 0.2-fold higher). However, the introduction of Exos-siPIK3CA led to a significant decrease in p-Akt levels, reducing it to a near-null value. Moreover, when Exos-siPIK3CA was introduced, there was a substantial decrease in p-mTOR protein expression, lowering it to approximately 0.4-fold.

Shifting our focus to RKO cells **(Figure 3.5 A** and **B)**, comparing the control group to the Exos-

siPIK3CA treatment, we observed a more significant reduction in PI3K protein expression to 0.1-fold. Identically with HCT-15 cells, no bands were observed in the Western blot for Akt. In mTOR expression, we also verified an mTOR expression decreased to 0.7-fold when treated with Exos, and a more substantial reduction indicating a near-null decrease in mTOR expression, with Exos-siPIK3CA treatment.

Exos treatment also induced a slight increase in p-Akt protein expression, **(Figure 3.5 A** and **C),** (approximately 0.2-fold higher). However, when Exos-siPIK3CA was administered, p-Akt levels experienced a significant reduction, decreasing to approximately 0.3-fold. Mimicking the previous result, Exos treatment led to a slight increase in p-mTOR levels (approximately 0.3-fold change higher), although the introduction of Exos-siPIK3CA resulted in a moderate decrease in p-mTOR expression, reducing it to approximately 0.2-fold.

Both HCT-15 and RKO cells exhibited reduced PI3K expression when treated with Exos-siPIK3CA, with RKO cells showing the most pronounced response. In terms of mTOR expression, both cell lines displayed a significant reduction, approaching near-null levels in mTOR protein expression. Concerning phosphorylated proteins, p-Akt levels in HCT-15 cells were dramatically reduced to near-null values, while p-mTOR levels saw significant decreases. In RKO cells, both p-Akt and p-mTOR levels were also markedly reduced, with p-Akt reaching a null value.

Interestingly, Zhang J *et al*. [118] reported that when bone marrow stromal cells (BMSCs) were incubated with only hiPS-MSC-Exos resulted in a significant increase in Akt phosphorylation protein, indicating that the PI3K/Akt signaling in BMSCs was activated by the exosomes. However, the upregulation of p-Akt in BMSCs by the exosomes was significantly impaired after the BMSCs were cultured with a PI3K inhibitor (LY294002; 10 μM), also in line with our results **(Figure 3.5 B** and **C)**.

Certainly, based on the provided analyses, it is evident that the results from both the PI3K, mTOR, p-Akt and p-mTOR experiments align coherently **(Figure 3.5 A, B,** and **C)**. These findings suggest that Exos-siPIK3CA treatment effectively downregulates the PI3K/Akt/mTOR signaling pathway, specifically affecting the active form of p-Akt and p-mTOR protein expression. This coherence in outcomes suggests a consistent impact of the treatment across the tested cellular parameters, indicating a synchronization in the cellular responses to these interventions in normal-form proteins and activated proteins.

3.5 Assessment of Cell Viability, Gene Expression and Cell Migration after Exos-siPIK3CA Treatment

The analysis presented in this research offers a closer look at the potential of Exos-siPI3K in *PIK3CA* gene expression, cell viability, and migratory potential in the respective cell lines **(Figure 3.6)**. The migration of cancer cells to distant sites in the body illustrates a major difficulty in the effectiveness of cancer therapies.

Assessing the migratory potential and motility of cells is instrumental in assessing the efficacy of our approach, against metastasis behaviour in cells.

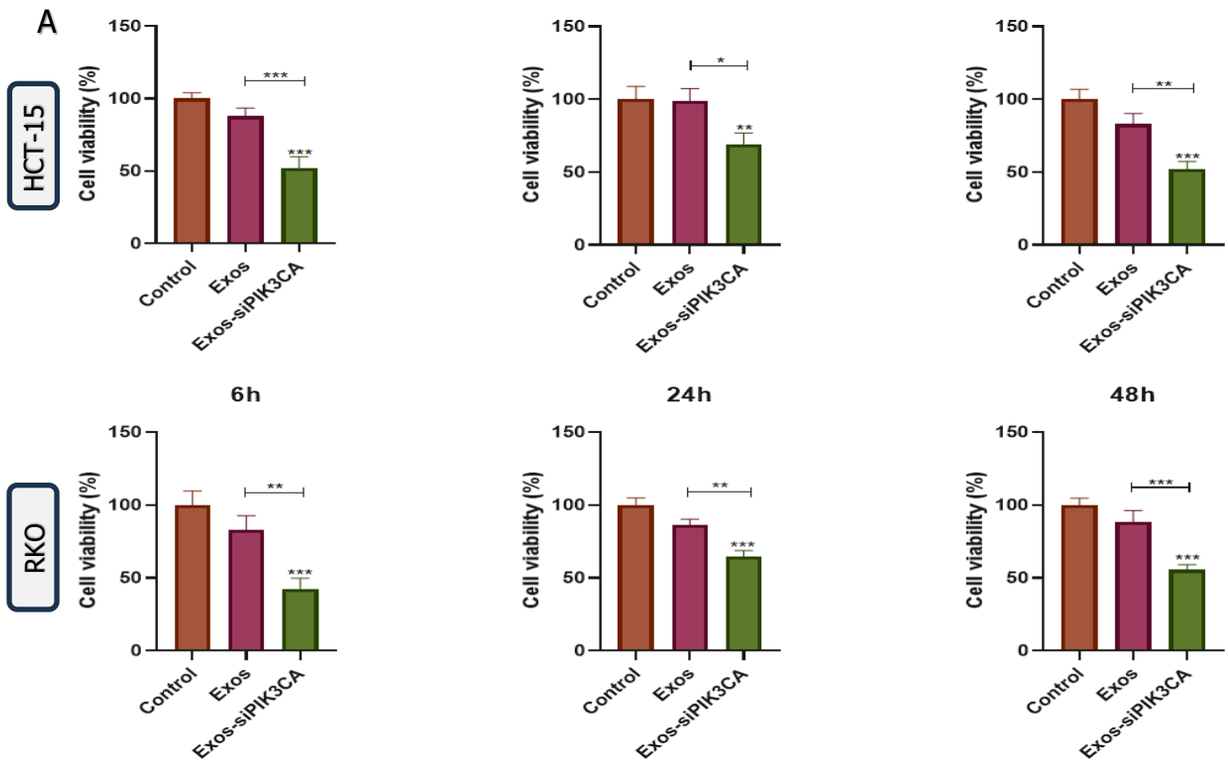

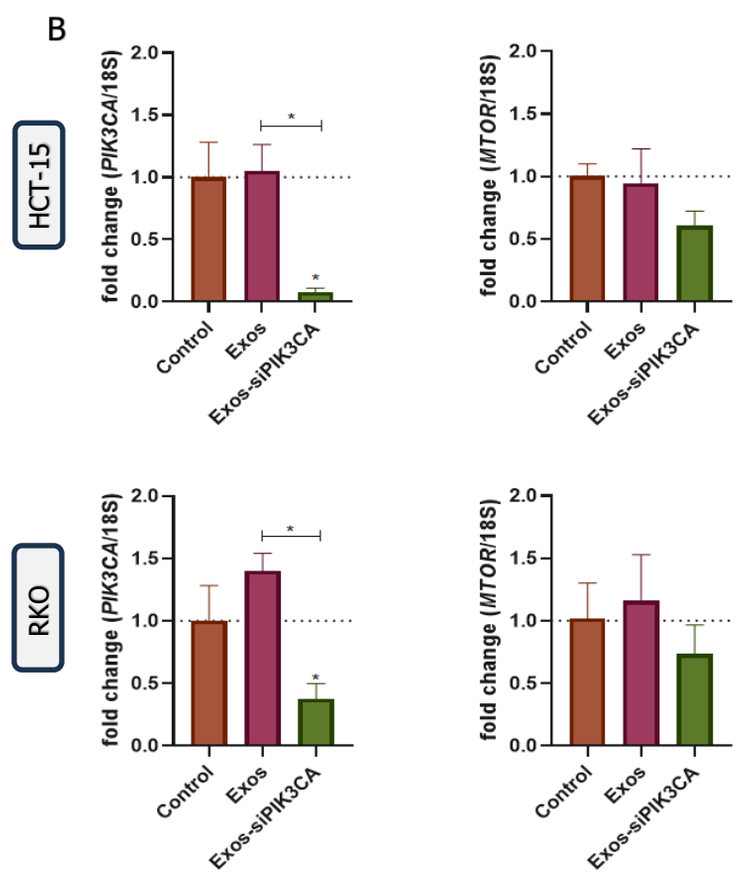

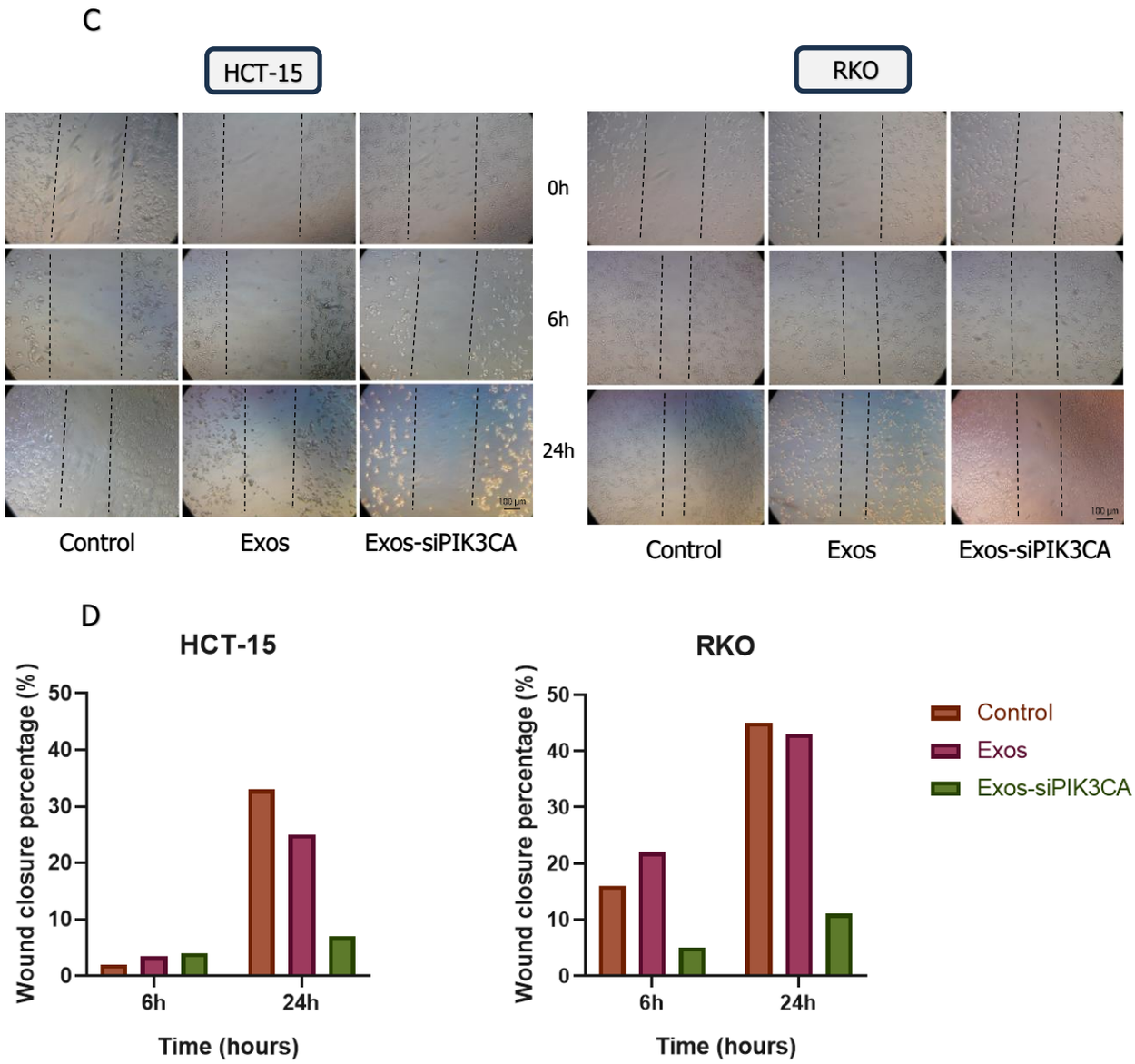

Figure 3.6 Effect of Exos-siPIK3CA on cell viability, gene expression and cell migration: (A) Assessment of HCT-15 and RKO cellular viability treated with Exos-siPIK3CA over time (6 h, 24 h and 48 h). For each time point, viability was estimated by MTT assay. Data from the MTT assay is expressed as the percentage ± SD of three independent experiments. Two-way ANOVA indicates statistically significant differences within the group assessed by Sidak's post-test and denoted as follows: ns $p > 0.05$, *$p \leq 0.05$ **$p \leq 0.01$, ***$p \leq 0.001$ and ****$p \leq 0.0001$. **(B)** Effect of Exos-siPIK3CA on the knockdown of *PIK3CA* and MTOR mRNA expression in HCT-15 and RKO cells. Non-treated cells were used as control and the 18S as the housekeeping gene. Data is representative of one independent assay with similar results. Two-way ANOVA indicates statistically significant differences within the group assessed by Sidak's post-test and denoted as follows: ns $p>0.05$ and *$p\leq0.05$. **(C)** Effect of Exos-siPIK3CA on the migration of HCT-15 and RKO cells throughout time (6 h and 24 h). Scale bar: 100 µm. **(D)** Quantitative analysis of wound closure percentage over time.

HCT-15 and RKO cells were treated with Exos-siPIK3CA and after 6 h, 24 h and 48 h the MTT assay was performed. The results, presented in **(Figure 3.6 A)**, show a decrease in cellular viability to 38.3 ± 3.2% for HCT-15 ($p \leq 0.001$), and 32.1 ± 4.21% for RKO ($p \leq 0.001$) at 6 h, compared to non-treated cells. Interestingly, it is for the shorter transfection period (6 h) that the effect is more pronounced, and it is possible to see a cellular recovery at 24 h with cellular viability at 62.2 ± 4.1% ($p \leq 0.01$) and 65.4 ± 5.1% ($p \leq 0.001$) for HCT-15 and RKO, respectively.

Moreover, a slight decrease of cellular viability at 48 h for the HCT-15 and RKO cells was observed reaching 52.6 ± 5.2% ($p \leq 0.001$) and 49.2 ± 3.5% ($p \leq 0.001$), respectively. Since for all the time points Exos condition did not promote significant effects ($p > 0.05$), it is possible to conclude that the decrease in cell viability is only stimulated by the siPIK3CA action.

Silva *et al*. [88] reported similar findings to our study. In their investigation involving treatment with exosomes loaded with a siRNA-targeting *PIK3CA*, they observed a significant reduction in cellular viability (6 h) for MDA-MB-231 and MDA-MB-453 cell lines, with viability decreasing to 52.3 ± 7.7% and 42.7 ± 1.2%, respectively. Notably, the most substantial and rapid response was achieved at the 6 h time point, outperforming the response at higher time points.

The data from the RT-PCR **(Figure 3.6 B**) clearly reveals that the effects of Exos-siPIK3CA treatment on *PIK3CA* and *MTOR* gene expressions are mostly similar between both cells. In HCT-15 cells, the treatment with Exos-siPIK3CA led to a remarkable downregulation in both *PI3K* and *mTOR* gene expressions. The *PIK3CA* gene expression exhibited a substantial reduction of 93% ($p \leq 0.05$), while mTOR expression showed a moderate decrease of 63%, though statistical significance was not observed ($p > 0.05$). A similar trend was observed in RKO cells, with a notable reduction in *PIK3CA* expression to nearly 35% ($p \leq 0.05$). Additionally, *MTOR* expression decreased to 65%, though, similar to HCT-15 cells, statistical significance was not reached ($p > 0.05$).

This observation aligns well with the findings of Silva *et al.* [88] and Xu *et al.* [120]. Silva *et al.* [88] achieved an impressive 85% silencing of the *PIK3CA* gene, while Xu *et al.* [120] recorded a significant 65% reduction in *PAK4* gene expression within their respective cell lines following exosome treatment with siRNA.

To study even further the impact of *PIK3CA* depletion, we analysed the dynamics of wound healing and cellular migration in HCT-15 and RKO cells. We employed an *in vitro* methodology to examine the influence of Exos-siPIK3CA on cancer cell migration. HCT-15 and RKO cells were seeded, subjected to scratch wounds, treated with Exos-siPIK3CA and monitored at various time points (0 h, 6 h, and 24 h) as depicted in **Figure 3.6 C** and **D**. Visual inspection of the results revealed a noteworthy distinction. While the gap in the non-treated group progressively reduced over time, the Exos-siPIK3CA treated cells did not exhibit the same degree of closure. Quantitative analysis was conducted by measuring the gap areas (using imageJ) and calculating the percentage of wound closure for control, Exos, and Exos-siPIK3CA transfected cells for the previously referred time intervals, as presented in **Figure 3.6 C** and **D**. The findings demonstrated a reduced capacity for wound closure in the transfected cells treated with Exos-siPIK3CA when compared to the control group at all time points. Particularly, the 24 h time point yielded the most pronounced results. Non-transfected cells showed a recovery of 33.2% and 44.7% of the gap area in HCT-15 and RKO, respectively, while Exos-siPIK3CA treated cells displayed a significantly lower recovery of only 6.4% and 11.9%. Furthermore, the Exos

condition and non-transfected cells produced similar results. Wang *et al.* [119] also observed a comparable outcome when exosomes, isolated from HEK-293t cells and loaded with TRPP2-siRNA, led to a notable reduction in the migration speed of human FaDu cells, in contrast to non-transfected cells. Silva *et al.* [88] achieved similar findings in TNBC cells, using the same siRNA-targeting *PIK3CA*, noting a substantial decrease in wound closure capacity for the transfected cells in comparison to the control group across all three time points at 24 h, 48 h, and 72 h. Therefore, these results support the conclusion that Exos-*siPIK3CA* effectively inhibited the in vitro migration capacity of HCT-15 and RKO cells.

Collectively, Exos-siPIK3CA electroporation effectively targets the *PIK3CA* gene in both cell lines. Initially, Exos-siPIK3CA promotes a substantial reduction in cell viability, as evidenced by MTT assay results for both cell types. Furthermore, the RT-PCR analysis indicates a higher and a rapidly *PI3K* knockdown in both cells. When considering cell migration and drawing from these compelling findings, it becomes evident that Exos-siPIK3CA treatment significantly reduces the migratory capabilities of HCT-15 and RKO cells in *in vitro* settings.

3.6 A Comparative Analysis of Lipofectamine vs Exosomes in siPIK3CA delivery

In order to understand the advantages of the application of exosomes as nanocarriers, **Table 3.1** compares the MTT, RT-PCR and Western Blot results obtained with Lipo-siPIK3CA and with Exos-siPIK3CA treatment.

Table 3.1: Comparison of the effect on cellular viability, protein expression and gene knockdown promoted by Lipo-siPIK3CA and Exos-siPIK3CA on HCT-15 and RKO cells.

Cellular line	Experiment	Lipo-siPIK3CA	Exo-siPIK3CA
HCT-15	Cell Viability	17.8% (72 h)	48.2% (6 h)
		54.2% (24 h)	62.2% (24 h)
	Western Blot	0% (72 h)	15.1% (6h)
	RT-PCR	25.2% (72 h)	7.2% (24 h)
RKO	Cell Viability	32.1% (72 h)	38.3% (6 h)
		57.5% (24 h)	65.4% (24 h)
	Western Blot	17.2% (72 h)	3.1% (6 h)
	RT-PCR	30.1% (72 h)	37.4% (24 h)

In **Table 3.1**, we notice a clear trend in how much each strategy impacts both cell types. While the Lipo-siPIK3CA (72 h) approach indeed induces the most substantial cellular viability decrease, resulting in reductions of 17% and 32% in HCT-15 and RKO cell viability, respectively, it is worth highlighting the impressive performance of Exos-siPIK3CA. Remarkably, this strategy manages to approach these levels of effectiveness within 6 h period. Even at the 24 h mark, where signs of recovery start to manifest in the Exos-siPIK3CA results, the disparities from Lipo-siPIK3CA remain marginal.

For instance, Silva *et al.* [88] reported even more promising results with Exos-siPIK3CA treatment at 6 h period, achieving a substantial 50% reduction in TNBC cell viability, surpassing the Lipo-siPIK3CA treatment by nearly 30%.

In the context of Western Blot analysis, we observed slight variations between the two treatment strategies. In the case of HCT-15, the Exos-siPIK3CA treatment resulted in a notable 15% in PI3K protein expression within a brief 6 h period, although the Lipo-siPIKCA approach exhibited a value of 0%, signifying null protein expression after an extended 72 h incubation. On the other hand, for RKO, the Lipo-siPIK3CA treatment yielded a 17% PI3K protein expression within 72 h, while the Exos-siPIK3CA approach displayed a minimal 3% PI3K expression, reaching near null protein expression after a 6 h transfection.

In line with our findings, Xu *et al.* [120] also achieved comparable results in the Western blot assay. When contrasted with Lipofectamine treatment, PANC-1-Exo demonstrated superior knockdown efficiency ($p < 0.01$) at an equivalent siPAK4 dosage of 30 nM.

Moving to the RT-PCR results, the Exos-siPI3K delivery strategy consistently revealed a higher knockdown effect in PAM elements mRNA expression compared to the Lipo-siPI3K approach. With HCT-15 cells reaching 7% *PIK3CA* expression and RKO reaching 37% for the time point of 6 h.

These findings correspond with the observations made by Silva *et al* [88] and Xu *et al*. [120], who reported a faster and more efficient silencing of *PI3K* and *PAK4* genes in respective cell lines after exosome-based delivery within a 4 h incubation, as opposed to lipofectamine transfection.

These outcomes provide compelling evidence for the effectiveness of Exos-siPI3K in mediating *siPIK3CA* delivery to HCT-15 and RKO cells. This is achieved by facilitating the formation of the RISC complex and subsequent mRNA cleavage. The key to this success appears to lie in the exosomes themselves, which function as highly efficient carriers, effectively bypassing endosomal degradation and clearance mechanisms. This advantage allows them to reach CRC cells with greater efficacy compared to the lipofectamine method.

This implies that exosomes serve as protective shields for siRNA, enabling a faster and more substantial impact. Silva *et al* [88] and Xu *et al*. [120], reported similar findings when delivering siRNA targeting in exosomes to TNBC and pancreatic cancer, respectively, achieving a greater decrease in cellular viability compared to lipofectamine-delivered siRNA.

Collectively, the outcomes of the table strongly endorse the application of exosomes as ideal and efficient *siPIK3CA* nanocarriers. Moreover, the Exos-siPIK3CA treatment demonstrates a more significant and quicker impact than the Lipo-siPIK3CA approach. This is likely attributed to the more efficient internalization of exosomes, as reported in the literature [82,83,84]. Lipofectamine's reliance on complex formation between siRNA and cationic lipids could expose siRNA to extracellular nucleases, potentially leading to degradation [73,74,75]. Conversely, exosomes, with their high biocompatibility, better mimicry of the plasma membrane, and cholesterol composition, offer superior siRNA protection and promote increased uptake.

Nevertheless, more studies are warranted to understand the effect of Exos-siPIK3CA on migration, protein expression, and cellular recovery beyond different and higher time points, as these aspects may guide the need for multiple dosing strategies.

4. Conclusion and Future Perspectives

The main goal of this research was to investigate the application of siRNA in suppressing *PIK3CA* expression, a key component of the PI3K/Akt/mTOR pathway implicated in various cellular processes such as motility, metabolism, growth, proliferation, and migration. Dysregulation of this pathway is a common occurrence in CRC. To evaluate the effectiveness of siRNA in silencing *PIK3CA* and its impact on the PI3K/Akt/mTOR pathway, we focused on two CRC cell lines, which carry distinct *PIK3CA* mutations: E545K (exon 9), as observed in HCT-15 cells, and H1047R (exon 20), as identified in RKO cells. In addition, CRC *PIK3CA* mutations are generally associated with KRAS mutations with RKO presenting WT gene and HCT-15 having a mutation in (38G > A). In this study, we explored the efficacy of two siPIK3CA delivery strategies, Lipofectamine and Exosomes due to their established efficacy.

Firstly, we demonstrated that the Lipofectamine-based delivery of siPIK3CA effectively reduces cellular viability in both HCT-15 and RKO cells. Notably, the highest concentration (50 nM) and the extended incubation time (72 h) led to the most substantial decrease in cell viability. These results align with previous studies and suggest the potential of siPIK3CA to target the PAM pathway effectively.

In addition, RT-PCR and Western Blot analysis revealed that siPIK3CA led to a transient knockdown, resulting in decreased PI3K protein and gene expression. The evaluation also indicated a reduction in mTOR levels. Both mRNA and protein levels of the PAM pathway were partially inhibited, in HCT and RKO cells, following Lipo-siPIK3CA transfection.

Collectively, these results validate the biological activity of siPIK3CA in vitro, leading to the reduction of mRNA and protein expression in the PAM pathway, as well as a decrease in cellular viability. Lipofectamine successfully delivered *PIK3CA* into the CRC cells, allowing the formation of the RISC complex and inhibiting the PAM pathway.

In the second phase of this study, exosomes were isolated from two non-tumorigenic cell lines HEK-293t. The Exosomes were characterized with the appropriate size by NTA and DLS, slightly negative zeta potential and were positive for the presence of CD9, CD81 and CD63. Furthermore, explored the use of exosomes as carriers for siPIK3CA. This approach proved highly efficient, leading to a rapid and significant reduction in cell viability in both cell lines. The most striking aspect of Exos-siPIK3CA was its ability to achieve near-null protein expression in a remarkably short 6 h period. Furthermore, RT-PCR and Western Blot analysis, revealed that Exos-siPIK3CA induced a more substantial decrease in *PIK3CA* and *MTOR* gene expression, further confirming the efficiency of this delivery strategy in mediating *PIK3CA* delivery. The results were consistent with both protein and gene expression, reinforcing the reliability and synchronization of the cellular responses to the Exos-siPIK3CA treatment.

In addition, we explored the impact of this therapy on cell migration. Our findings demonstrated a significant reduction in the migratory capabilities of both HCT-15 and RKO cells when treated with Exos-siPIK3CA, highlighting the potential of this approach to not only reduce mRNA and protein knockdown but also hinder the metastatic properties of cancer cells. These findings highlight the potential of exosomes as superior nanocarriers for siRNA delivery, with benefits including rapid action and greater overall efficacy.

While promising, these preliminary results necessitate further investigation. To gain a comprehensive understanding, it is imperative to delve deeper into the mechanisms underlying cellular death, protein and gene expression and migration capacity in response to exosome-based delivery. The specific mechanisms of exosome-based siRNA delivery also require more extensive exploration.

This study has provided significant insights into the role of siRNA in inhibiting *PIK3CA* expression and disrupting the PAM pathway, and it also highlights various directions for future research.

While optimizing siRNA concentrations and evaluating longer time points is essential for a comprehensive assessment of CRC recovery and transfection efficiency, exploring the distinct *PIK3CA* mutations in different CRC may yield valuable insights into the effectiveness of siPIK3CA across other different cancer types.

Additionally, the study opens exciting possibilities for siRNA-based cancer therapy, particularly through exosome-based delivery. To maximize the potential, further research is needed to fine-tune and optimize exosome-based siRNA delivery. This entails investigating various exosome sources, cargo loading methods, and dosing regimens to enhance delivery efficiency.

In-depth studies are required to elucidate the molecular mechanisms by which *PIK3CA*, delivered by exosomes, exerts its effects. A deeper understanding of these mechanisms can lead to more precise targeting of cancer cells. The translation of siRNA-based therapies from laboratory studies to clinical settings is a significant challenge. Future research should focus on developing safe and effective clinical protocols for using Exos-siPIK3CA in patients with CRC. Furthermore, research should aim to investigate and mitigate any potential off-target effects or adverse reactions associated with siRNA-based therapies, especially when applied in clinical settings.

Investigating the potential of combining Exos-siPIK3CA with other therapeutic modalities, such as chemotherapy or immunotherapy, could lead to synergistic effects in cancer treatment. For instance, combining siRNA treatments with traditional chemotherapeutics could enhance response in gene, protein expression and cell viability in CRC cells carrying the *PIK3CA* mutation.

Moreover, considering a multiple-targeting siRNA approach, simultaneously targeting *PI3K, Akt, and mTOR* genes within the PAM pathway, has the potential to disrupt existing feedback loops and enhance the inhibition of critical cancer-related pathways. Extending the analysis of gene knockdown and cell migration to

a broader set of cell lines and animal models can provide a comprehensive understanding of the potential benefits of Exos-siPIK3CA in inhibiting cancer metastasis.

In conclusion, this research successfully validated the use of siRNA in suppressing *PIK3CA* expression, thereby disrupting the PAM pathway in CRC. Additionally, the study provides valuable insights into the role of *PIK3CA* mutations in therapeutic resistance. The utilization of exosomes as carriers for *PIK3CA* revealed a more rapid and robust effect than traditional lipofectamine transfection, offering a promising alternative for siRNA delivery. This work lays the foundation for the development of an exosome-based siRNA delivery system, opening avenues for further research and eventual clinical applications in the fight against CRC.

5. REFERENCES

1. Dagenais, G. R., et al. (2020). Variations in common diseases, hospital admissions, and deaths in middle-aged adults in 21 countries from five continents (PURE): a prospective cohort study. *The Lancet, 395*(10226), 785-794.

2. Torre, L. A., et al. (2016). Global Cancer Incidence and Mortality Rates and Trends Update. *Cancer Epidemiology Biomarkers & Prevention, 25*(1), 16-27.

3. Siegel, R. L., K. D. Miller, and A. Jemal (2020). Cancer statistics, 2020. *CA: A Cancer Journal for Clinicians, 70*(1), 7-30.

4. Yancik, R. (2005). Population aging and cancer: A cross-national concern. *Cancer Journal, 11*(6), 437-441.

5. Xi Y, Xu P. (2021). Global colorectal cancer burden in 2020 and projections to 2040. *Transl Oncol, 14*(10), 101174.

6. Dekker E., Tanis P.J., Vleugels J.L.A., Kasi P.M., Wallace M.B. (2019). Colorectal cancer. *Lancet, 394*, 1467–1480.

7. Currais, P., Mão de Ferro, S., Areia, M., Marques, I., Mayer, A., & Dias Pereira, A. (2021). Should Colorectal Cancer Screening in Portugal Start at the Age of 45 Years? A Cost-Utility Analysis. *GE Portuguese Journal of Gastroenterology, 28*(5), 311–318.

8. World Health Organization. International Agency of Research of Cancer.

9. Markowitz SD, Bertagnolli MM. (2009). Molecular origins of cancer: Molecular basis of colorectal cancer. *New England Journal of Medicine, 361*(8), 2449-2460.

10. Compton, C. C., & Greene, F. L. (2004). The staging of colorectal cancer: 2004 and beyond. *CA Cancer Journal for Clinicians, 54*(6), 295-308.

11. Rosen RD, Sapra A. (2023). TNM Classification. In: *StatPearls [Internet]*. Treasure Island (FL): StatPearls Publishing;.

12. Dienstmann R, Salazar R, Tabernero J. (2018). Molecular subtypes and the evolution of treatment decisions in metastatic colorectal cancer. *American Society of Clinical Oncology Educational Book, 38*, 231-238.

13. Campbell. (2018) 18.5 Figure 18.26. *Biology: A Global Approach*.

14. Hansen, T. F., Qvortrup, C., & Pfeiffer, P. (2021). Angiogenesis Inhibitors for Colorectal Cancer. A Review of the Clinical Data. *Cancers, 13*(5), 1031.

15. Fruman, D. A., et al. (2017). The PI3K Pathway in Human Disease. *Cell, 170*(4), 605-635.

16. Muzny, D. M., et al. (2012). Comprehensive molecular characterization of human colon and rectal cancer. *Nature, 487*(7407), 330-337.

17. Engelman JA. (2009). Targeting PI3K signaling in cancer: opportunities, challenges, and limitations. *Nature Reviews Cancer, 9*(8), 550-562.

18. Manning BD, Cantley LC. (2007). AKT/PKB signaling: navigating downstream. *Cell, 129*(7), 1261-1274.

19. Vanhaesebroeck B, Stephens L, Hawkins P. (2012). PI3K signaling: the path to discovery and understanding. *Nature Reviews Molecular Cell Biology, 13*(3), 195-203.

20. Manning BD, Toker A. (2017). AKT/PKB signaling: navigating the network. *Cell, 169*(3), 381-405.

21. Fruman DA, Meyers RE, Cantley LC. (1998). Phosphoinositide kinases. *Annual Review of Biochemistry, 67*, 481-507.

22. Alessi DR, James SR, Downes CP, et al. (1997). Characterization of a 3-phosphoinositide-dependent protein kinase which phosphorylates and activates protein kinase Bα. *Current Biology, 7*(4), 261-269.

23. Sarbassov DD, Guertin DA, Ali SM, Sabatini DM. (2005). Phosphorylation and regulation of Akt/PKB by the rictor-mTOR complex. *Science, 307*(5712), 1098-1101.

24. Zhao L, Vogt PK. (2008). Class I PI3K in oncogenic cellular transformation. *Oncogene, 27*(41), 5486–5496.

25. Cantrell DA. (2001). Phosphoinositide 3-kinase signaling pathways. *Journal of Cell Science, 114*(Pt 8), 1439–145.

26. Kim C, Lee JH, Ko JH, Chinnathambi A, Alharbi SA, Shair OHM, et al. (2019). Formononetin Regulates Multiple Oncogenic Signaling Cascades and Enhances Sensitivity to Bortezomib in a Multiple Myeloma Mouse Model. *Biomolecules, 9*(7), 262.

27. Castellano E, Downward J. (2011) RAS Interaction with PI3K: More Than Just Another Effector Pathway. *Genes Cancer, 2*(3), 261–74.

28. Ikenoue T, Kanai F, Hikiba Y, Obata T, Tanaka Y, Imamura J, et al. (2005). Functional analysis of PIK3CA gene mutations in human colorectal cancer. *Cancer Res, 65*(11), 4562–7.

29. Jiang W, He T, Liu S, Zheng Y, Xiang L, Pei X, et al. (2018). The PIK3CA E542K and E545K mutations promote glycolysis and proliferation via induction of the β-catenin/SIRT3 signaling pathway in cervical cancer. *J Hematol Oncol, 11*(1), 139.

30. Croessmann S, Sheehan JH, Lee KM, Sliwoski G, He J, Nagy R, et al. (2018). C2 Domain Deletions Hyperactivate Phosphoinositide 3-kinase (PI3K), Generate Oncogene Dependence, and Are Exquisitely Sensitive to PI3K. *Clin Cancer Res, 24*(6), 1426–35.

31. Jin J, Shi Y, Zhang S, Yang S. (2020). PIK3CA mutation and clinicopathological features of colorectal cancer: a systematic review and Meta-Analysis. *Acta Oncol, 59*(1), 66–74.

32. Atanasova VS, Riedl A, Strobl M, Flandorfer J, Unterleuthner D, Weindorfer C, et al. (2023). Selective Eradication of Colon Cancer Cells Harboring PI3K and/or MAPK Pathway Mutations in 3D Culture by Combined PI3K/AKT/mTOR Pathway and MEK Inhibition. *Int J Mol Sci, 24*(2), 1668.

33. Sirico M, D'Angelo A, Gianni C, Casadei C, Merloni F, De Giorgi U. (2023). Current State and Future Challenges for PI3K Inhibitors in Cancer Therapy. *Cancers (Basel), 15*(3), 703.

34. Yu M, Chen J, Xu Z, Yang B, He Q, Luo P, et al. (2023). Development and safety of PI3K inhibitors in cancer. *Arch Toxicol, 97*(3), 635–50.

35. Schram et al. (2018). A phase Ib dose-escalation and expansion study of the oral MEK inhibitor pimasertib and PI3K/MTOR inhibitor voxtalisib in patients with advanced solid tumours. *British Journal of Cancer,, 119*(12), 1471–1476.

36. X Do et al. (2015). Biomarker-driven phase 2 study of MK-2206 and selumetinib (AZD6244, ARRY-142886) in patients with colorectal cancer. *Investigational New Drugs,, 33*(3), 720–728.

37. Yokota et al. (2014) Phase I clinical trial of DS-7423, an oral PI3K/MTOR dual inhibitor, in Japanese patients with advanced solid tumors. *Annals of Oncology, 25*(Supplement 4), iv146–iv164.

38. Capano et al. (2021) MEN1611 in combination with cetuximab: Targeting PIK3CA mutations in RAS-wild-type patient-derived colorectal cancer xenografts. *Annals of Oncology, [Volume 32].

39. Fakih et al. (2023) A study to evaluate the safety and tolerability of the covalent phosphoinositide-3-kinase (PI3K)-alpha Inhibitor, TOS-358, in adult subjects with select solid tumors. *Part 2 (Clinical Trials and Late-Breaking Research); Apr 14-19; Orlando, FL. Philadelphia (PA): AACR; Cancer Res 2023;83(8_Suppl).

40. Zhang Y, Kwok-Shing Ng P, Kucherlapati M, Chen F, Liu Y, Tsang YH, et al. (2017) A Pan-Cancer Proteogenomic Atlas of PI3K/AKT/mTOR Pathway Alterations. *Cancer Cell, 31*(6), 820–32.e3.

41. Kumar, A., & Purohit, R. (2013). Cancer-associated E17K mutation causes rapid conformational drift in AKT1 pleckstrin homology (PH) domain. PLoS ONE, 8(5), e64364.

42. Parikh, C., Janakiraman, V., Wu, W. I., Foo, C. K., Kljavin, N. M., Chaudhuri, S., et al. (2012). Disruption of PH-kinase domain interactions leads to oncogenic activation of AKT in human cancers. Proceedings of the National Academy of Sciences of the United States of America, 109(47), 19368–73.

43. Park, E. S., Rabinovsky, R., Carey, M., Hennessy, B. T., Agarwal, R., Liu, W., et al. (2010). Integrative analysis of proteomic signatures, mutations, and drug responsiveness in the NCI 60 cancer cell line set. Molecular Cancer Therapeutics, 9(2), 257–67.

44. Basu, A., & Lambring, CB. (2021). Akt Isoforms: A Family Affair in Breast Cancer. Cancers (Basel), 13(14), 3445.

45. Altomare, D. A., & Testa, J. R. (2005). Perturbations of the AKT signaling pathway in human cancer. Oncogene, 24(50), 7455–64.

46. Yang, W. L., Wu, C. Y., Wu, J., & Lin, H. K. (2010). Regulation of Akt signaling activation by ubiquitination. Cell Cycle, 9(3), 487–97.

47. Fusco, N., Sajjadi, E., Venetis, K., Gaudioso, G., Lopez, G., Corti, C., et al. (2020). Alterations and Their Role in Cancer Management: Are We Making Headway on Precision Medicine? Genes (Basel), 11(7), 719.

48. Vidotto, T., Melo, C. M., Lautert-Dutra, W., Chaves, LP, Reis, RB, & Squire, JA. (2023). Pan-cancer genomic analysis shows hemizygous PTEN loss tumors are associated with immune evasion and poor outcome. Scientific Reports, 13(1), 5049.

49. Jin, J., Shi, Y., Zhang, S., & Yang, S. (2020). PIK3CA mutation and clinicopathological features of colorectal cancer: a systematic review and Meta-Analysis. Acta Oncologica, 59(1), 66–74.

50. Jiang, Y., Liu, X. Q., Rajput, A., Geng, L., Ongchin, M., Zeng, Q., et al. (2011). Phosphatase PRL-3 is a direct regulatory target of TGFbeta in colon cancer metastasis. Cancer Research, 71(1), 234–44.

51. Puzio-Kuter, A. M., Castillo-Martin, M., Kinkade, C. W., Wang, X., Shen, TH, Matos, T., et al. (2009). Inactivation of p53 and Pten promotes invasive bladder cancer. Genes & Development, 23(6), 675–80.

52. Fire, A., et al. (1998). Potent and specific genetic interference by double-stranded RNA in Caenorhabditis elegans. Nature, 391(6669), 806-811.

53. Hannon, G. J. (2002). RNA interference. Nature, 418(6894), 244-251.

54. Lee, Y., et al. (2003). The nuclear RNase III Drosha initiates microRNA processing. Nature, 425(6956), 415-419.

55. Meister, G., & Tuschl, T. (2004). Mechanisms of gene silencing by double-stranded RNA. Nature, 431(7006), 343-349.

56. Lee, R. C., et al. (1993). The C. elegans heterochronic gene lin-4 encodes small RNAs with antisense complementarity to lin-14. Cell, 75(5), 843-854.

57. Lee, Y., et al. (2006). The role of PACT in the RNA silencing pathway. EMBO Journal, 25(3), 522-532.

58. Kim, V. N. (2005). MicroRNA biogenesis: coordinated cropping and dicing. Nature Reviews Molecular Cell Biology, 6(5), 376-385.

59. Elbashir, S. M., et al. (2001). Duplexes of 21-nucleotide RNAs mediate RNA interference in cultured mammalian cells. Nature, 411(6836), 494-498.

60. Reynolds, A., et al. (2004). Rational siRNA design for RNA interference. Nature Biotechnology, 22(3), 326-330.

61. Bernstein E, et al.(2001) Role of a bidentate ribonuclease in the initiation step of RNA interference. Nature.;409(6818):363-366.

62. Hammond SM, et al.(2001) Argonaute2, a link between genetic and biochemical analyses of RNAi. Science.;293(5532):1146-1150.

63. Bartel DP.(2009) MicroRNAs: target recognition and regulatory functions. Cell.;136(2):215-233.

64. Doench JG, Sharp PA.(2004) Specificity of microRNA target selection in translational repression. Genes Dev.;18(5):504-511.

65. Jackson AL, et al. (2006) Widespread siRNA "off-target" transcript silencing mediated by seed region sequence complementarity. RNA.;12(7):1179-1187.

66. Birmingham A, et al. (2006) 3' UTR seed matches, but not overall identity, are associated with RNAi off-targets. Nat Methods.;3(3):199-204.

67. Meister G, et al. (2004) Mechanisms of gene silencing by double-stranded RNA. Nature. ;431(7006):343-349.

68. Davidson BL, McCray PB Jr.(2011) Current prospects for RNA interference-based therapies. Nat Rev Genet.;12(5):329-340.

69. Ui-Tei K, et al. (2004) Guidelines for the selection of highly effective siRNA sequences for mammalian and chick RNA interference. Nucleic Acids Res.;32(3):936-948.

70. Amarzguioui M, et al.(2006) Rational design and *in vitro* and *in vivo* delivery of Dicer substrate siRNA. Nat Protoc.;1(2):508-517.

71. Khvorova A, Reynolds A, Jayasena SD. (2003) Functional siRNAs and miRNAs exhibit strand bias. Cell.;115(2):209-216.

72. Matranga C, et al. (2005) Passenger-strand cleavage facilitates the assembly of siRNA into Ago2-containing RNAi enzyme complexes. Cell.;123(4):607-620.

73. Schwarz DS, et al.(2003) Asymmetry in the assembly of the RNAi enzyme complex. Cell.;115(2):199-208.

74. Jackson AL, et al. (2006) Position-specific chemical modification of siRNAs reduces "off-target" transcript silencing. RNA.;12

75. Peer D, et al. (2007) Nanocarriers as an emerging platform for cancer therapy. Nat Nanotechnol.;2(12):751-760.

76. Zabner J, et al. (2015) Safety and efficacy of repeated monthly doses of aerosolized AAV5-siRNA complexes in Rhesus monkeys. Mol Ther. ;23(11):1712-1722.

77. Kanasty R, et al. (2013)Delivery materials for siRNA therapeutics. Nat Mater.;12(11):967-977.

78. Yin H, et al. (2014) Non-viral vectors for gene-based therapy. Nat Rev Genet;15(8):541-555.

79. Yhee JY, et al. Smart nanoparticles for drug delivery (2018) Boundaries and opportunities. Chem Eng Sci. ;177:322-332.

80. Chakraborty C, et al. (2011) Nanoparticle-mediated siRNA delivery for cancer therapy: Progress, challenges, and perspectives. Pharm Res.;28(6):1463-1475.

81. Torchilin VP. Recent advances with liposomes as pharmaceutical carriers.(2005) Nat Rev Drug Discov.;4(2):145-160.

82. Yáñez-Mó M, Siljander PR-M, Andreu Z, et al. (2015) Biological properties of extracellular vesicles and their physiological functions. J Extracell Vesicles;4(1):27066.

83. Colombo M, Raposo G, Théry C. (2014) Biogenesis, secretion, and intercellular interactions of exosomes and other extracellular vesicles. Annu Rev Cell Dev Biol.;30:255-289.

84. van Niel G, D'Angelo G, Raposo G. (2018) Shedding light on the cell biology of extracellular vesicles. Nat Rev Mol Cell Biol;19(4):213-228.

85. Robbins PD, Morelli AE. (2014) Regulation of immune responses by extracellular vesicles. Nat Rev Immunol;14(3):195-208.

86. Wu M, et al. (2021) Macropinocytosis and endosomal membrane recycling in amoeba: Parallels to macrophages. Int J Mol Sci;22(15):8033.

87. Groot Kormelink T, et al. (2016) Prerequisites for the analysis and sorting of extracellular vesicle subpopulations by high-resolution flow cytometry. Cytometry A;89(2):135-147.

88. Silva R, et al. (2022) Exosome-based delivery of RNAi leads to breast cancer inhibition, Journal of Drug Delivery Science and Technology, Volume 78, 2022, 103931, ISSN 1773-2247.

89. György B, et al. (2011) Membrane vesicles, current state-of-the-art: Emerging role of extracellular vesicles. Cell Mol Life Sci.;68(16):2667-2688.

90. Wiklander OPB, et al. (2015) Extracellular vesicle *in vivo* biodistribution is determined by cell source, route of administration and targeting. J Extracell Vesicles;4:26316.

91. Hood JL, et al. (2011) Externalization of autophagy-related proteins and elements of the endosomal system within extracellular vesicles: Differentiating mechanisms of release and uptake. Cancer Res.;71(23):6747-6755.

92. Wang C., Li N., Li Y., Hou S., Zhang W., Meng Z., Wang S., Jia Q., Tan J., Wang R., et al.(2022) Engineering a HEK-293T exosome-based delivery platform for efficient tumor-targeting chemotherapy/internal irradiation combination therapy. J. Nanobiotechnol;20:247.

93. Fath, et al. Exosome-based strategies for diagnosis and therapy of glioma cancer,(2022). Cancer Cell International. Volume 22.

94. Kooijmans SAA, et al. (2013) Electroporation-induced siRNA precipitation obscures the efficiency of siRNA loading into extracellular vesicles. J Control Release.;172(1):229-238.

95. Haney MJ, et al. (2015)Exosomes as drug delivery vehicles for Parkinson's disease therapy. J Control Release.;207:18-30.

96. Ohno S, et al. (2013) Systemically injected exosomes targeted to EGFR deliver antitumor microRNA to breast cancer cells. Mol Ther;21(1):185-191.

97. Tian Y, et al. (2014) A doxorubicin delivery platform using engineered natural membrane vesicle exosomes for targeted tumour therapy. Biomaterials;35(7):2383-2390.

98. Lee J, Lee H, Goh U, Kim J, Jeong M, Lee J. et al. (2016) Cellular engineering with membrane fusogenic liposomes to produce functionalized extracellular vesicles. *ACS Appl Mater Interfaces*; 8:6790–5.

99. Cui G-h, Guo H-d, Li H, Zhai Y, Gong Z-b, Wu J. et al. (2019) RVG-modified exosomes derived from mesenchymal stem cells rescue memory deficits by regulating inflammatory responses in a mouse model of Alzheimer's disease. Immun Ageing;16:10.

100. Lamichhane TN, et al. (2015) Emerging roles for extracellular vesicles in tissue engineering and regenerative medicine. Tissue Eng Part B Rev;21(1):45-54.

101. Livak, K. J.; Schmittgen, T. D.(2001) Analysis of Relative Gene Expression Data Using Real-Time Quantitative PCR and the 2−ΔΔCT Method. Methods, 25 (4), 402–408.

102. Cardarelli, F., Digiacomo, L., Marchini, C., Amici, A., Salomone, F., Fiume, G., Rossetta, A., Gratton, E., Pozzi, D., & Caracciolo, G. (2016). The intracellular trafficking mechanism of Lipofectamine-based transfection reagents and its implication for gene delivery. Scientific reports, 6, 25879.

103. Zhao, L., & Vogt, P. K. (2008). Class I PI3K in oncogenic cellular transformation. Oncogene, 27(41), 5486–5496.

104. Wang J, Zhu X, Xu X, et al. (2017) PIK3CA mutations and downstream effector p-mTOR expression: implication for prognostic factors and therapeutic targets in triple negative breast cancer. Int J Clin Exp Pathol;10(7):7682-7691.

105. Vaidya, S., Jeengar, M. K., Wadaan, M. A., Mahboob, S., Kumar, P., Reece, L. M., Bathula, S. R., & Dutta, M. (2022). Design and In Vitro Evaluation of Novel Cationic Lipids for siRNA Delivery in Breast Cancer Cell Lines. Evidence-based complementary and alternative medicine : eCAM, 9231641.

106. Weigelt, B.; Downward, J. (2011) PIK3CA Mutation, but Not PTEN Loss of Function, Determines the Sensitivity of Breast Cancer Cells to MTOR Inhibitory Drugs.

107. Dufour M., Dormond-Meuwly A., Pythoud C., Demartines N., Dormond O.(2013) Reactivation of AKT signaling following treatment of cancer cells with PI3K inhibitors attenuates their antitumor effects. Biochem. Biophys. Res. Commun;438:32–37.

108. Valentino, J. D., Elliott, V. A., Zaytseva, Y. Y., Rychahou, P. G., Mustain, W. C., Wang, C., Gao, T., & Evers, B. M. (2012). Novel small interfering RNA cotargeting strategy as treatment for colorectal cancer. Surgery, 152(2), 277–285.

109. Yansheng Liu, Andreas Beyer, Ruedi Aebersold,(2016) On the Dependency of Cellular Protein Levels on mRNA Abundance, Cell,Volume 165, Issue 3,Pages 535-550, ISSN 0092-8674.

110. Zhou, X., Xie, F., Wang, L., Zhang, L., Zhang, S., Fang, M., & Zhou, F. (2020). The function and clinical application of extracellular vesicles in innate immune regulation. Cellular & molecular immunology, 17(4), 323–334

111. Théry C, Witwer KW, Aikawa E, et al. (2018) Minimal information for studies of extracellular vesicles; a position statement of the International Society for Extracellular Vesicles and update of the MISEV2014 guidelines. J Extracell Vesicles;7(1)

112. Ferreira, D., Santos-Pereira, et al. (2023). Exosomes modified with anti-MEK1 siRNA lead to an effective silencing of triple negative breast cancer cells. Biomaterials advances, 154, 213643.

113. Mendt M, Kamerkar S, Sugimoto H, et al. (2018) Generation and testing of clinical-grade exosomes for pancreatic cancer. JCI Insight;3(8)

114. Zaborowski, M. P., Balaj, L., Breakefield, X. O., & Lai, C. P. (2015). Extracellular Vesicles: Composition, Biological Relevance, and Methods of Study. Bioscience, 65(8), 783-797.

115. Didiot MC, Hall LM, Coles AH, et al.(2016) Exosome-mediated Delivery of Hydrophobically Modified siRNA for Huntingtin mRNA Silencing. Mol Ther;24(10)

116. Munagala R, Aqil F, Jeyabalan J, et al (2021). Exosome-mediated delivery of RNA and DNA for gene therapy. Cancer Lett;505:58-72.

117. Kugeratski FG, Hodge K, Lilla S, et al.(2021) Quantitative proteomics identifies the core proteome of exosomes with syntenin-1 as the highest abundant protein and a putative universal biomarker. Nat Cell Biol;23(6):631-641

118. Zhang, J., Liu, X., Li, H. et al. (2016). Exosomes/tricalcium phosphate combination scaffolds can enhance bone regeneration by activating the PI3K/Akt signaling pathway. Stem Cell Res Ther 7, 136 .

119. Wang, C., Chen, L., Huang, Y., Li, K., Jinye, A., Fan, T. (2019). Exosome delivered TRPP2 siRNA inhibits the epithelial mesenchymal transition of FaDu cells. Oncology Letters, 17, 1953-1961.

120. Xu, L., Faruqu, F. N., Lim, Y. M., Lim, et al. (2021). Exosome-mediated RNAi of PAK4 prolongs survival of pancreatic cancer mouse model after loco-regional treatment. Biomaterials, 264, 120369.

SUPPLEMENTARY INFORMATION

Appendix Figures

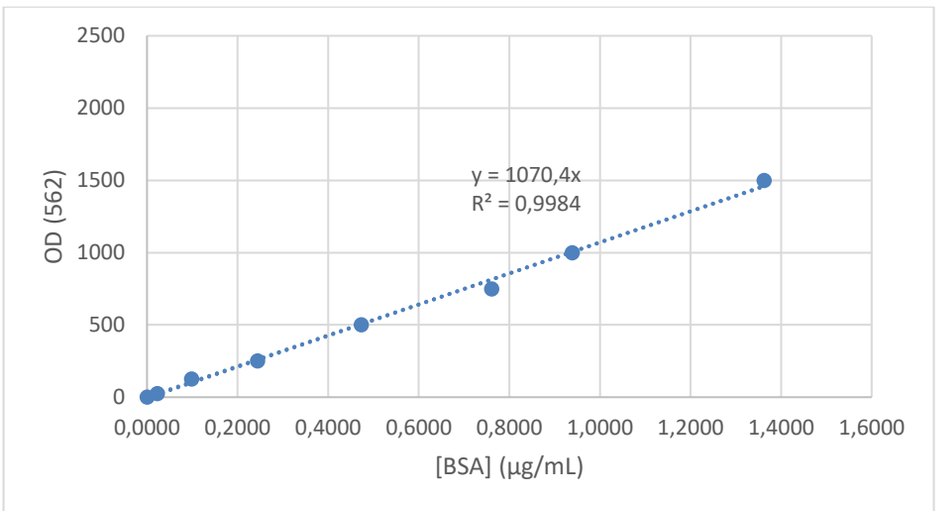

Figure A.1: Calibration curve applied for protein quantification with BCA protein assay kit.

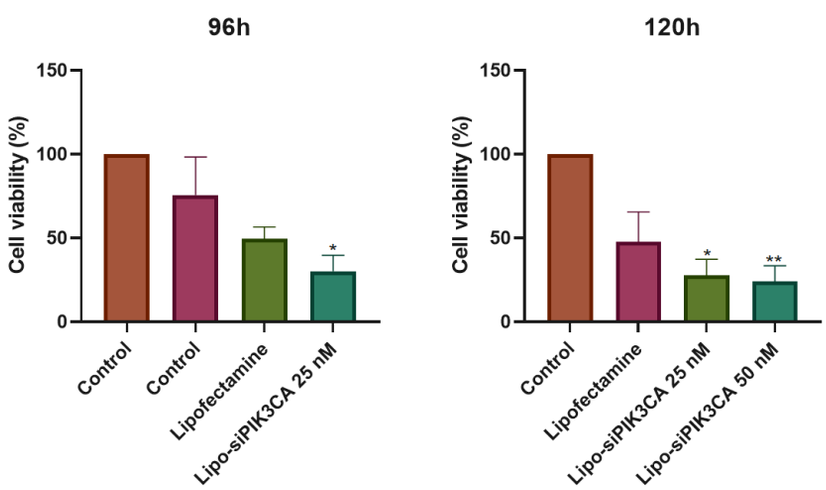

Figure A.2: Assessment of the cellular viability promoted by siPIK3CA: Evaluation of HCT-15 cellular viability treated with Lipofectamine and siPIK3CA (25 nM or 50 nM) over 96 h and 120 h. For each time point, viability was estimated by the MTT assay. All data is presented as the percentage of cell viability ± SD of three independent experiments. Two-way ANOVA indicates statistically significant: non-significant $p > 0.05$, *$p \leq 0.05$, **$p \leq 0.01$.

.